

# Ring Size Matters: Supramolecular Isomerism in Self-Assembled Redox-Active Tetra- and Hexaruthenium Macrocycles

Daniel Fink, Nicole Orth, Michael Linseis, Ivana Ivanović-Burmazović and Rainer F. Winter\*

D. Fink, Dr. M. Linseis, Prof. R. Winter

Fachbereich Chemie, Universität Konstanz

78457 Konstanz (Germany)

N. Orth, Prof. I. Ivanović-Burmazović

Department Chemie und Pharmazie, Friedrich-Alexander-Universität Erlangen-Nürnberg

91058 Erlangen (Germany)

## Supporting Information

### Experimental Procedures, Synthesis and Characterization Data

Methods and Materials .....	5
Electrochemical and Spectroelectrochemical Measurements.....	5
Computational Details: .....	6
Synthesis and Characterization.....	7
NMR Spectra .....	9
<b>Figure S1.</b> $^{31}\text{P}\{\text{H}\}$ NMR spectrum of macrocycle <b>2-TF</b> <sub>6</sub> , measured in C <sub>6</sub> D <sub>6</sub> . .....	9
<b>Figure S2.</b> $^{31}\text{P}\{\text{H}\}$ NMR spectrum of macrocycle <b>2-TF</b> <sub>4</sub> , measured in C <sub>6</sub> D <sub>6</sub> . .....	9
<b>Figure S3.</b> $^1\text{H}$ NMR spectrum of macrocycle <b>2-TF</b> <sub>6</sub> , measured in C <sub>6</sub> D <sub>6</sub> . ....	10
<b>Figure S4.</b> $^1\text{H}$ NMR spectrum of macrocycle <b>2-TF</b> <sub>4</sub> , measured in C <sub>6</sub> D <sub>6</sub> . ....	10
<b>Figure S5.</b> $^{13}\text{C}\{\text{H}\}$ NMR spectrum of macrocycle <b>2-TF</b> <sub>6</sub> , measured in C <sub>6</sub> D <sub>6</sub> . ....	11
<b>Figure S6.</b> $^{13}\text{C}\{\text{H}\}$ NMR spectrum of macrocycle <b>2-TF</b> <sub>4</sub> , measured in C <sub>6</sub> D <sub>6</sub> . ....	11
<b>Figure S7.</b> Excerpt from the DOSY spectrum of a mixture of the two macrocyclic isomers <b>2-TF</b> <sub>4</sub> (grey) and <b>2-TF</b> <sub>6</sub> (blue). ....	12
ESI MS .....	13
<b>Figure S8.</b> ESI Mass spectrum of macrocycle <b>2-TF</b> <sub>6</sub> (top), magnified [M- 2 P <sup>i</sup> Pr <sub>3</sub> ] <sup>2+</sup> peak with calculated isotopic pattern (bottom). .....	13
<b>Figure S9.</b> ESI Mass spectrum of macrocycle <b>2-TF</b> <sub>4</sub> (top), magnified M <sup>+</sup> peak with calculated isotopic pattern (bottom). .....	14

X-ray Crystallography .....	15
Compound 2-TF <sub>6</sub> : .....	15
<b>Figure S10.</b> Structure of macrocycle 2-TF <sub>6</sub> as the benzene dodecasolvate with atom numbering. Benzene solvate molecules as well as hydrogen atoms have been removed for reasons of clarity. Ellipsoids are drawn at a 50% probability level. ....	15
<b>Table S1.</b> Crystal data and structure refinement for macrocycle 2-TF <sub>6</sub> ·12 C <sub>6</sub> H <sub>6</sub> . ....	16
<b>Table S2.</b> Selected bond lengths [Å] for 2-TF <sub>6</sub> ·12 C <sub>6</sub> H <sub>6</sub> . ....	17
<b>Table S3.</b> Selected bond angles [°] for 2-TF <sub>6</sub> ·12 C <sub>6</sub> H <sub>6</sub> . ....	19
Compound 2-TF <sub>4</sub> : .....	23
<b>Figure S11.</b> Structure of macrocycle 2-TF <sub>4</sub> as the benzene tetrasolvate with atom numbering. Benzene solvate molecules as well as hydrogen atoms have been removed for clarity reasons. Ellipsoids are drawn at a 50% probability level. ....	23
<b>Table S4.</b> Crystal data and structure refinement for macrocycle 2-TF <sub>4</sub> ·4 C <sub>6</sub> H <sub>6</sub> . ....	24
<b>Table S5.</b> Selected bond lengths [Å] for 2-TF <sub>4</sub> ·4 C <sub>6</sub> H <sub>6</sub> . ....	25
<b>Table S6.</b> Selected bond angles [°] for 2-TF <sub>4</sub> ·4 C <sub>6</sub> H <sub>6</sub> . ....	26
Cyclic Voltammetry .....	28
Compound 2-TF <sub>6</sub> : .....	28
<b>Figure S12.</b> Cyclic voltammograms for the first composite wave of macrocycle 2-TF <sub>6</sub> at $v = 100$ mV/s (left) and at $v = 25, 50, 100, 200, 400, 600, 800, 1000$ mV/s (right) in CH <sub>2</sub> Cl <sub>2</sub> / <sup>n</sup> Bu <sub>4</sub> NBAr <sup>F24</sup> . ....	28
<b>Figure S13.</b> Cyclic voltammograms for the first two composite waves of macrocycle 2-TF <sub>6</sub> at $v = 100$ mV/s (left) and at $v = 25, 50, 100, 200, 400, 600, 800, 1000$ mV/s (right) in CH <sub>2</sub> Cl <sub>2</sub> / <sup>n</sup> Bu <sub>4</sub> NBAr <sup>F24</sup> . ....	28
<b>Table S7.</b> Data of the cyclovoltammetric measurements for macrocycle 2-TF <sub>6</sub> at different scan rates, measured in CH <sub>2</sub> Cl <sub>2</sub> / <sup>n</sup> Bu <sub>4</sub> NBAr <sup>F24</sup> . ....	29
<b>Figure S14.</b> Square wave voltammogram of macrocycle 2-TF <sub>6</sub> (left) with deconvolution (right), measured in CH <sub>2</sub> Cl <sub>2</sub> / <sup>n</sup> Bu <sub>4</sub> NBAr <sup>F24</sup> . ....	29
Compound 2-TF <sub>4</sub> : .....	30
<b>Figure S15.</b> Cyclic voltammograms for the first composite wave of macrocycle 2-TF <sub>4</sub> at $v = 100$ mV/s (left) and at $v = 25, 50, 100, 200, 400, 600, 800, 1000$ mV/s (right) in CH <sub>2</sub> Cl <sub>2</sub> / <sup>n</sup> Bu <sub>4</sub> NBAr <sup>F24</sup> . ....	30

<b>Figure S16.</b> Cyclic voltammograms for the first two composite waves of macrocycle <b>2-TF<sub>4</sub></b> at $v = 100$ mV/s (left) and at $v = 25, 50, 100, 200, 400, 600, 800, 1000$ mV/s (right) in $\text{CH}_2\text{Cl}_2/\text{nBu}_4\text{NBAr}^{\text{F}24}$ .....	30
<b>Table S8.</b> Data of the cyclovoltammetric measurements for macrocycle <b>2-TF<sub>4</sub></b> at different scan rates, measured in $\text{CH}_2\text{Cl}_2/\text{nBu}_4\text{NBAr}^{\text{F}24}$ .....	31
<b>Figure S17.</b> Square wave voltammogram of macrocycle <b>2-TF<sub>4</sub></b> (left) with deconvolution (right), measured in $\text{CH}_2\text{Cl}_2/\text{nBu}_4\text{NBAr}^{\text{F}24}$ .....	31
Spectroelectrochemistry .....	32
Compound 2-TF <sub>6</sub> : .....	32
<b>Figure S18.</b> Changes in the NIR (left) and mid-IR (Ru(CO)) (right) spectra of <b>2-TF<sub>6</sub></b> upon oxidation to <b>2-TF<sub>6</sub><sup>3+</sup></b> , measured in $\text{CH}_2\text{Cl}_2/\text{nBu}_4\text{NPF}_6$ (0.2 M, r. t.) .....	32
<b>Figure S19.</b> Changes in the NIR (left) and mid-IR (Ru(CO)) (right) spectra of <b>2-TF<sub>6</sub><sup>3+</sup></b> upon further oxidation to <b>2-TF<sub>6</sub><sup>6+</sup></b> , measured in $\text{CH}_2\text{Cl}_2/\text{nBu}_4\text{NPF}_6$ (0.2 M, r. t.) .....	32
<b>Figure S20.</b> Changes in the UV/Vis/NIR spectra of <b>2-TF<sub>6</sub></b> upon oxidation to <b>2-TF<sub>6</sub><sup>3+</sup></b> (left) and deconvolution (right), measured in $\text{CH}_2\text{Cl}_2/\text{nBu}_4\text{NPF}_6$ (0.2 M, r. t.) .....	32
<b>Figure S21.</b> Changes in the UV/Vis/NIR spectra upon further oxidation of <b>2-TF<sub>6</sub><sup>3+</sup></b> to <b>2-TF<sub>6</sub><sup>6+</sup></b> (left) and deconvolution (right), measured in $\text{CH}_2\text{Cl}_2/\text{nBu}_4\text{NPF}_6$ (0.2 M, r. t.) .....	33
Compound 2-TF <sub>4</sub> : .....	33
<b>Figure S22.</b> Changes in the NIR (left) and mid-IR (Ru(CO)) (right) spectra of <b>2-TF<sub>4</sub></b> upon oxidation to <b>2-TF<sub>4</sub><sup>2+</sup></b> , measured in $\text{CH}_2\text{Cl}_2/\text{nBu}_4\text{NPF}_6$ (0.2 M, r. t.) .....	33
<b>Figure S23.</b> Changes in the NIR (left) and mid-IR (Ru(CO)) (right) spectra upon further oxidation of <b>2-TF<sub>4</sub><sup>2+</sup></b> to <b>2-TF<sub>4</sub><sup>4+</sup></b> , measured in $\text{CH}_2\text{Cl}_2/\text{nBu}_4\text{NPF}_6$ (0.2 M, r. t.) .....	33
<b>Figure S24.</b> Changes in the UV/Vis/NIR spectra of <b>2-TF<sub>4</sub></b> upon oxidation to <b>2-TF<sub>4</sub><sup>2+</sup></b> (left) and deconvolution (right), measured in $\text{CH}_2\text{Cl}_2/\text{nBu}_4\text{NPF}_6$ (0.2 M, r. t.) .....	34
<b>Figure S25.</b> Changes in the UV/Vis/NIR spectra upon further oxidation of <b>2-TF<sub>4</sub><sup>2+</sup></b> to <b>2-TF<sub>4</sub><sup>4+</sup></b> (left) and deconvolution (right), measured in $\text{CH}_2\text{Cl}_2/\text{nBu}_4\text{NPF}_6$ (0.2 M, r. t.) .....	34
EPR Spectroscopy .....	35
Compound 2-TF <sub>6</sub> : .....	35
<b>Figure S26.</b> EPR spectra of <b>2-TF<sub>6</sub><sup>3+</sup></b> (left) and <b>2-TF<sub>6</sub><sup>6+</sup></b> (right) at room temperature. ....	35
Compound 2-TF <sub>4</sub> : .....	35
<b>Figure S27.</b> EPR spectra of <b>2-TF<sub>4</sub><sup>2+</sup></b> (left) and <b>2-TF<sub>4</sub><sup>4+</sup></b> (right) at room temperature. ....	35

DFT Calculations.....	36
<b>Figure S28.</b> Calculated geometry-optimized structures of the two isomeric model compounds <b>2-TF<sub>4</sub><sup>M<sub>e</sub></sup></b> (left) and <b>2-TF<sub>6</sub><sup>M<sub>e</sub></sup></b> (right).....	36
References .....	37

## Experimental Details

### Methods and Materials

All manipulations were done under purified nitrogen with dry, distilled and nitrogen-saturated solvents. All reagents were purchased from commercial sources and used without further purification.  $^1\text{H}$  NMR (400 MHz),  $^{13}\text{C}$  NMR (101 MHz) and  $^{31}\text{P}$  NMR (162 MHz) spectra were measured on a Bruker AvanceIII 400 spectrometer, and  $^1\text{H}$  NMR (600 MHz) and  $^{13}\text{C}$  NMR (151 MHz) spectra on a Bruker AvanceIII 600 spectrometer.  $\text{HRu}(\text{CO})\text{Cl}(\text{P}^{\text{i}}\text{Pr}_3)_2$ <sup>(1)</sup> and  $[\{\text{Ru}(\text{CO})\text{Cl}(\text{P}^{\text{i}}\text{Pr}_3)_2\}_2(\mu\text{-2,5-(CH=CH)}_2\text{-C}_4\text{H}_2\text{S}](\mathbf{1-T})$ <sup>(2)</sup> were prepared according to literature methods.

EPR spectra were obtained using an X-band tabletop spectrometer MiniScope MS 400 by magnettech GmbH. All measurements were performed at room temperature and the macrocycles were chemically oxidized using ferrocenium hexafluoroantimonate ( $\text{Cp}_2\text{FeSbF}_6$ ), acetylferrocenium hexafluoroantimonate ( ${}^{\text{Ac}}\text{Cp}_2\text{FeSbF}_6$ ) or 1,1'diacetylferrocenium hexafluoroantimonate ( ${}^{\text{Ac2}}\text{Cp}_2\text{FeSbF}_6$ ) as oxidizing agents.

Mass spectra were recorded on an UHR-ToF Bruker Daltonik (Bremen, Germany) maXis plus instrument, an ESI-quadrupole time-of-flight (qToF) mass spectrometer capable of resolution of at least 60.000 FWHM. Detection was done in the positive-ion mode with a 4.5 kV voltage supply. The drying gas ( $\text{N}_2$ ) was held at 180 °C and the spray gas was held at 20 °C. The spectrometer was calibrated with ESI-ToF Low Concentration Tuning Mix of Agilent prior to every measurement. All measurements were carried out using dichloromethane as solvent. Additional ESI-MS data was acquired on a Bruker micrOTOF II mass spectrometer (Bruker, Billerica, MA, USA).

X-Ray diffraction analysis was performed on a STOE IPDS-II diffractometer equipped with a graphite-monochromated radiation source ( $\lambda = 0.71073 \text{ \AA}$ ) and an image plate detection system at 100.15 K. Using Olex2,<sup>(3)</sup> the structures were solved with the SIR2004<sup>(4)</sup> structure solution program using Direct Methods or the ShelXT<sup>(5)</sup> structure solution program using Intrinsic Phasing and refined with the ShelXL<sup>(6)</sup> refinement package using Least Squares minimization. Hydrogen atoms were introduced at their calculated positions. Structure plots were made with the Platon program.

### Electrochemical and Spectroelectrochemical Measurements

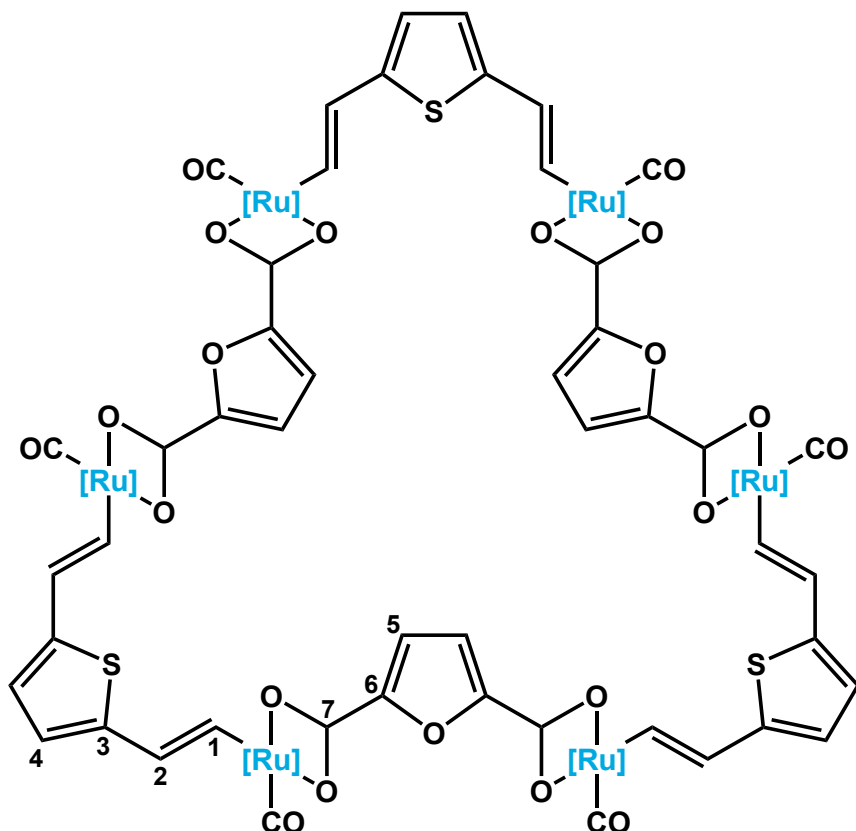
All electrochemical experiments were performed in a home-built cylindrical vacuum-tight one-compartment cell. A spiral-shaped Pt wire and an Ag wire as the counter and reference electrodes are sealed into glass capillaries that are introduced via Quickfit screws at opposite sides of the cell. A platinum electrode is introduced as the working electrode through the top port via a Teflon screw cap with a suitable fitting. It is polished with first 1  $\mu\text{m}$  and the 0.25  $\mu\text{m}$  diamond pastes (Buehler-Wirtz) before measurements. The cell can be attached to a conventional Schlenk line via a side arm equipped with a Teflon screw valve and allows experiments to be performed under an atmosphere of argon with approximately 5 mL of analyte solution.  ${}^{\text{n}}\text{Bu}_4\text{NPF}_6$  and  ${}^{\text{n}}\text{Bu}_4\text{NAr}^{\text{F}}$  were used as the supporting electrolytes. Referencing was done with addition of equimolar amount of cobaltocenium hexafluorophosphate as an internal standard to the analyte solution after all data of interest had been acquired. Representative sets of scans were repeated with the added standard. The final referencing was done against the ferrocene/ferrocenium ( $\text{Cp}_2\text{Fe}^{0/+}$ ) redox couple with  $E_{1/2} \text{ Cp}_2\text{Co}^{+/0} = -1330 \text{ mV vs. Cp}_2\text{Fe}^{0/+}$ . Electrochemical data were acquired with a computer-controlled BASi potentiostat. The OTTLE cell was also home-built and comprises of a Pt-mesh working and counter electrode and a thin silver wire as a pseudoreference electrode sandwiched between the  $\text{CaF}_2$  windows of a conventional liquid IR cell. Its design follows that of Hartl et al.<sup>(7)</sup> The working electrode is positioned in the centre of the spectrometer beam. For every measurement, a Wenking POS 2 potentiostat by Bank Elektronik - Intelligent Controls GmbH was used. FT-IR spectra were recorded using a Bruker Tensor II FT-IR spectrometer. UV/Vis/NIR spectra were obtained on a TIDAS fiberoptic diode array spectrometer (combined MCS UV/NIR and PGS NIR instrumentation) from j&m Analytik AG.

### **Computational Details:**

The ground state electronic structures of complexes **2-TF<sub>4</sub>** and **2-TF<sub>6</sub>** were calculated by density functional theory (DFT) methods using the Gaussian 09 program packages.<sup>(8)</sup> Open shell systems were calculated by the unrestricted Kohn-Sham approach (UKS). Geometry optimization followed by vibrational analysis was performed in solvent media. Solvent effects were described by the polarizable continuum model (PCM) with standard parameters for 1,2-dichloroethane.<sup>(9)</sup> The quasirelativistic Wood-Boring small-core pseudopotentials (MWB)<sup>(10)</sup> and the corresponding optimized set of basis functions for Ru<sup>(11)</sup> and 6-31G(d) polarized double- $\zeta$  basis sets<sup>(12)</sup> for the remaining atoms were employed together with the Perdew, Burke, Ernzerhof exchange and correlation functional (PBE0)<sup>(13)</sup>. The GaussSum program package was used to analyze the results,<sup>(14)</sup> while the visualization of the results was performed with the Avogadro program package.<sup>(15)</sup> Graphical representations of molecular orbitals were generated with the help of GNU Parallel<sup>(16)</sup> and plotted using the vmd program package<sup>(17)</sup> in combination with POV-Ray.<sup>(18)</sup>

## Synthesis and Characterization

**Macrocyclic 2-TF<sub>6</sub>:** A solution of 15.6 mg (0.100 mmol, 1.0 eq) of furan-2,5-dicarboxylic acid and 27.6 mg (0.200 mmol, 2.0 eq) of K<sub>2</sub>CO<sub>3</sub> in 30 ml of MeOH was slowly added to a solution of 110.4 mg (0.100 mmol, 1.0 eq) of **1-T** in 20 ml of CH<sub>2</sub>Cl<sub>2</sub>. The resulting yellow suspension was stirred for 12 h at room temperature. The solvents were removed under reduced pressure and the residue was taken up in 20 ml of CH<sub>2</sub>Cl<sub>2</sub>. Insoluble material was removed via centrifugation. CH<sub>2</sub>Cl<sub>2</sub> was removed *in vacuo* and the resulting yellow solid was washed with *n*-hexane. Yield: 80 mg (67%)



$$[\text{Ru}] = \text{Ru}(\text{P}^i\text{Pr}_3)_2$$

**<sup>1</sup>H NMR** (600 MHz, C<sub>6</sub>D<sub>6</sub>): δ in ppm = 8.78 (d, 6H, <sup>3</sup>J<sub>H,H</sub> = 15.2 Hz, H<sub>(1)</sub>), 7.15 (s, 6H, H<sub>(5)</sub>), 6.70 (d, 6H, <sup>3</sup>J<sub>H,H</sub> = 15.2 Hz, H<sub>(2)</sub>), 6.45 (s, 6H, H<sub>(4)</sub>), 2.36 - 2.23 (m, 36H, PHC(CH<sub>3</sub>)<sub>2</sub>), 1.28 - 1.22 (m, 216H, PHC(CH<sub>3</sub>)<sub>2</sub>)

**<sup>31</sup>P{<sup>1</sup>H} NMR** (162 MHz, C<sub>6</sub>D<sub>6</sub>): δ in ppm = 37.47 (s, P<sup>i</sup>Pr<sub>3</sub>)

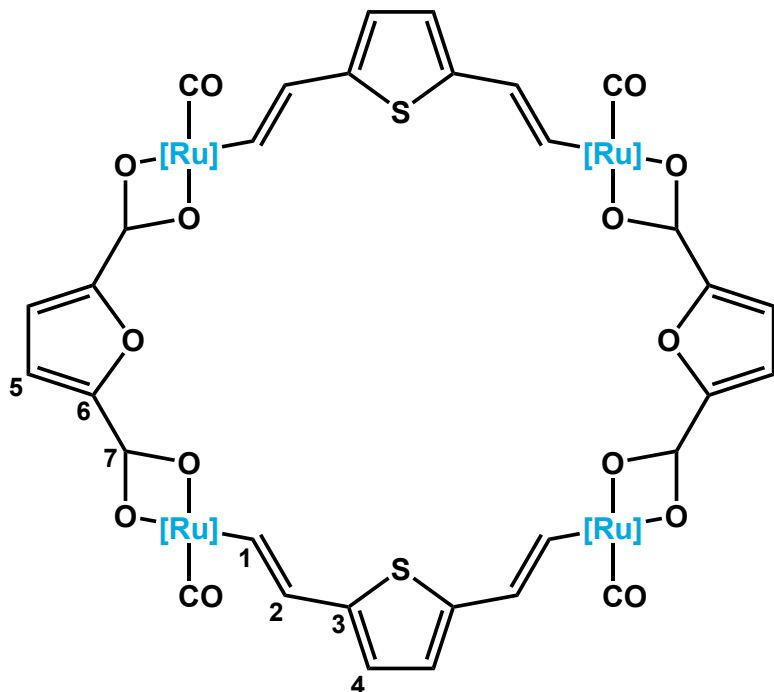
**<sup>13</sup>C{<sup>1</sup>H} NMR** (151 MHz, C<sub>6</sub>D<sub>6</sub>): δ in ppm = 209.1 (t, <sup>2</sup>J<sub>C,P</sub> = 13.5 Hz, RuCO), 168.4 (s, C<sub>(7)</sub>), 158.4 (s, C<sub>(1)</sub>), 150.2 (s, C<sub>(6)</sub>), 144.7 (s, C<sub>(3)</sub>), 129.8 (s, C<sub>(2)</sub>), 116.8 (s, C<sub>(4)</sub>), 116.3 (s, C<sub>(5)</sub>), 25.0 (vt, <sup>1</sup>J<sub>C,P</sub> = 9.5 Hz, PHC(CH<sub>3</sub>)<sub>2</sub>), 20.0 (s, PHC(CH<sub>3</sub>)<sub>2</sub>), 19.8 (s, PHC(CH<sub>3</sub>)<sub>2</sub>)

**IR** (CH<sub>2</sub>Cl<sub>2</sub>): 1906 cm<sup>-1</sup> (ν<sub>C=O</sub>)

**UV/Vis** (CH<sub>2</sub>Cl<sub>2</sub>): λ<sub>max</sub> = 390 nm, ε = 76200 M<sup>-1</sup>cm<sup>-1</sup>

**ESI MS** (CH<sub>2</sub>Cl<sub>2</sub>): 3562.0808 m/z ([M]<sup>+</sup>, calculated: 3562.0816 m/z), 1781.5322 m/z ([M]<sup>2+</sup>, calculated: 1781.5444 m/z)

**Macrocycle 2-TF<sub>4</sub>:** A solution of 10.0 mg **2-TF<sub>6</sub>** in 0.5 ml C<sub>6</sub>D<sub>6</sub> was stirred for 168 h at 35 °C. The solvent was removed *in vacuo* and the resulting yellow solid was subsequently washed with small amounts of *n*-hexane. Yield: 9.1 mg (91%)



**<sup>1</sup>H NMR** (600 MHz, C<sub>6</sub>D<sub>6</sub>): δ in ppm = 8.79 (d, 4H, <sup>3</sup>J<sub>H,H</sub> = 15.2 Hz, H<sub>(1)</sub>), 6.97 (s, 4H, H<sub>(5)</sub>), 6.87 (d, 4H, <sup>3</sup>J<sub>H,H</sub> = 15.2 Hz, H<sub>(2)</sub>), 6.49 (s, 4H, H<sub>(4)</sub>), 2.31 - 2.36 (m, 24H, PHC(CH<sub>3</sub>)<sub>2</sub>), 1.24 - 1.33 (m, 144H, PHC(CH<sub>3</sub>)<sub>2</sub>)

**<sup>31</sup>P{<sup>1</sup>H} NMR** (162 MHz, C<sub>6</sub>D<sub>6</sub>): δ in ppm = 38.00 (s, P*i*Pr<sub>3</sub>)

**<sup>13</sup>C{<sup>1</sup>H} NMR** (151 MHz, C<sub>6</sub>D<sub>6</sub>): δ in ppm = 209.9 (t, <sup>2</sup>J<sub>C,P</sub> = 13.1 Hz, RuCO), 168.8 (s, C<sub>(7)</sub>), 157.0 (t, <sup>2</sup>J<sub>C,P</sub> = 11.9 Hz, C<sub>(1)</sub>), 150.0 (s, C<sub>(6)</sub>), 144.8 (s, C<sub>(3)</sub>), 131.2 (s, C<sub>(2)</sub>), 117.9 (s, C<sub>(4)</sub>), 117.0 (s, C<sub>(5)</sub>), 25.2 (vt, <sup>1</sup>J<sub>C,P</sub> = 9.7 Hz, PHC(CH<sub>3</sub>)<sub>2</sub>), 20.0 (s, PHC(CH<sub>3</sub>)<sub>2</sub>), 19.8 (s, PHC(CH<sub>3</sub>)<sub>2</sub>)

**IR** (CH<sub>2</sub>Cl<sub>2</sub>): 1905 cm<sup>-1</sup> (ν<sub>C≡O</sub>)

**UV/Vis** (CH<sub>2</sub>Cl<sub>2</sub>): λ<sub>max</sub> = 391 nm, ε = 51200 M<sup>-1</sup>cm<sup>-1</sup>

**ESI MS** (CH<sub>2</sub>Cl<sub>2</sub>): 2375.7184 m/z ([M]<sup>+</sup>, calculated: 2375.7259 m/z), 1187.8595 m/z ([M]<sup>2+</sup>, calculated: 1187.8627 m/z)

## NMR Spectra

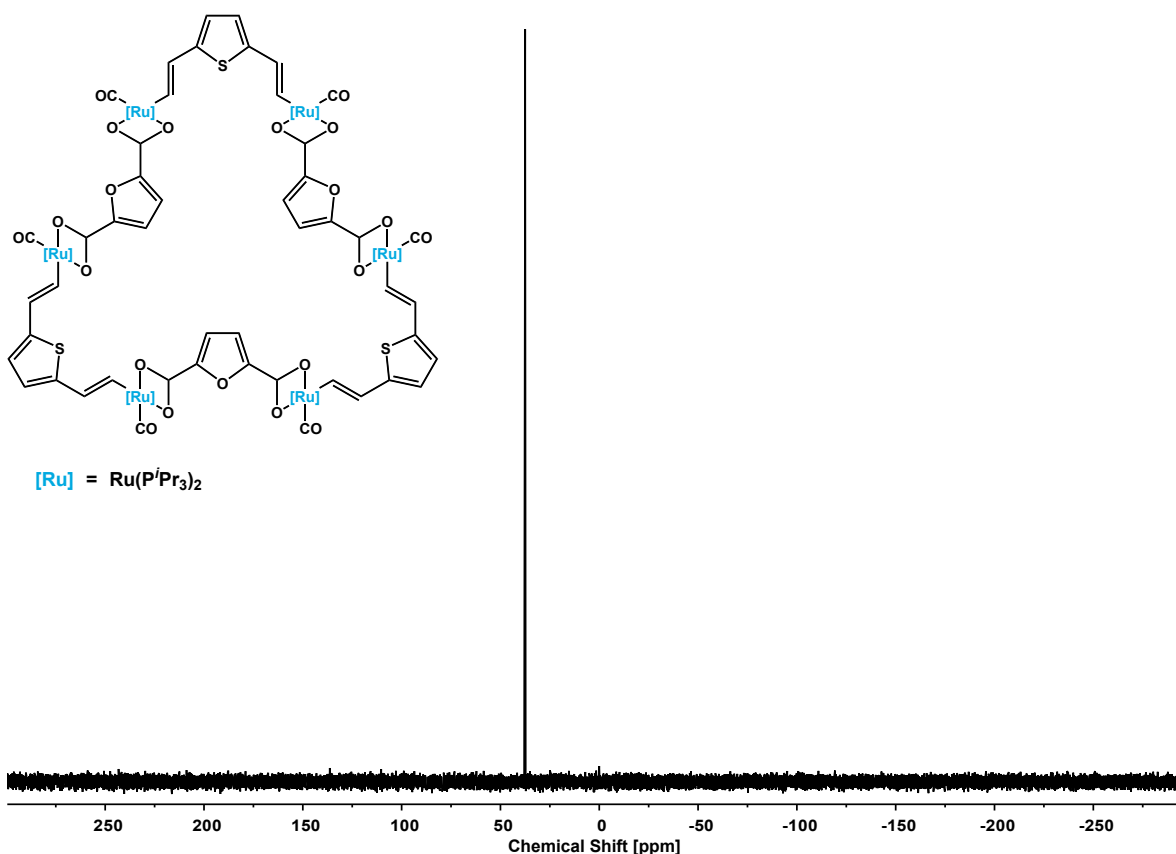


**Figure S1.** <sup>31</sup>P{<sup>1</sup>H} NMR spectrum of macrocycle **2-TF<sub>6</sub>**, measured in C<sub>6</sub>D<sub>6</sub>.

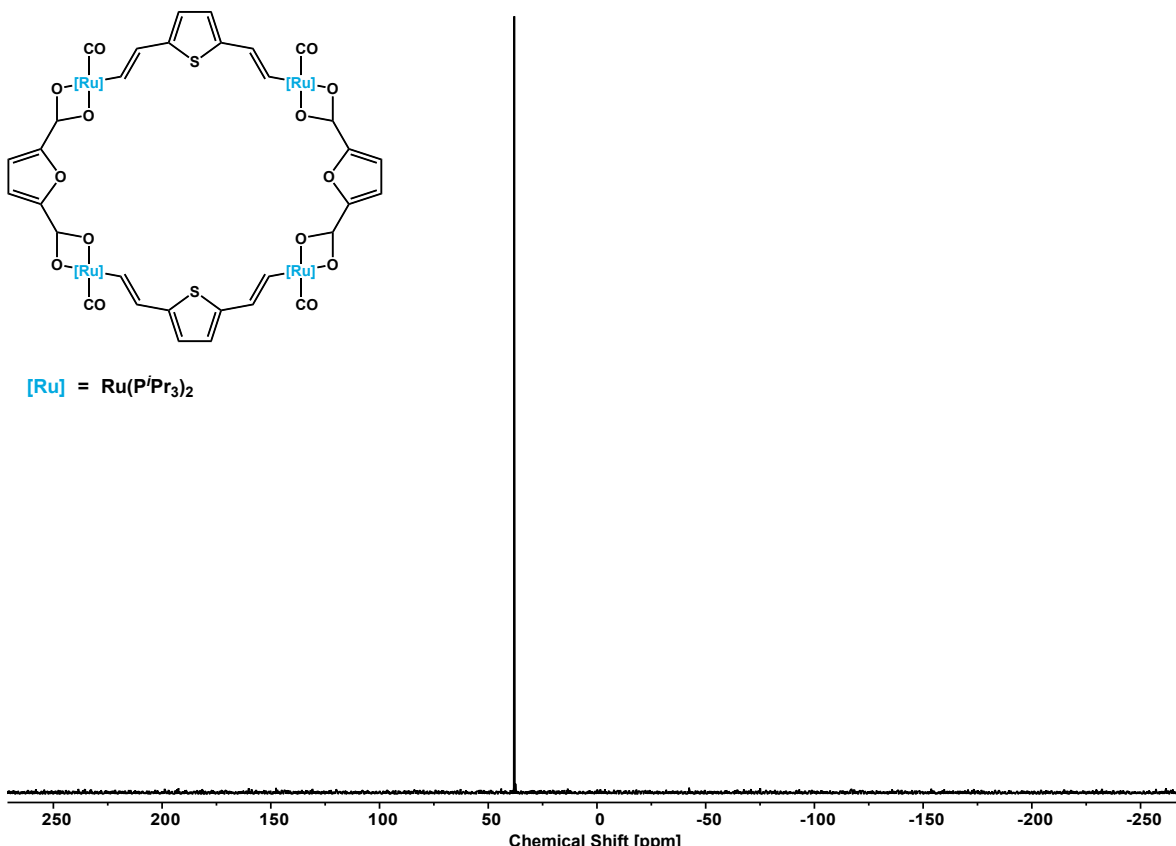


**Figure S2.** <sup>31</sup>P{<sup>1</sup>H} NMR spectrum of macrocycle **2-TF<sub>4</sub>**, measured in C<sub>6</sub>D<sub>6</sub>.

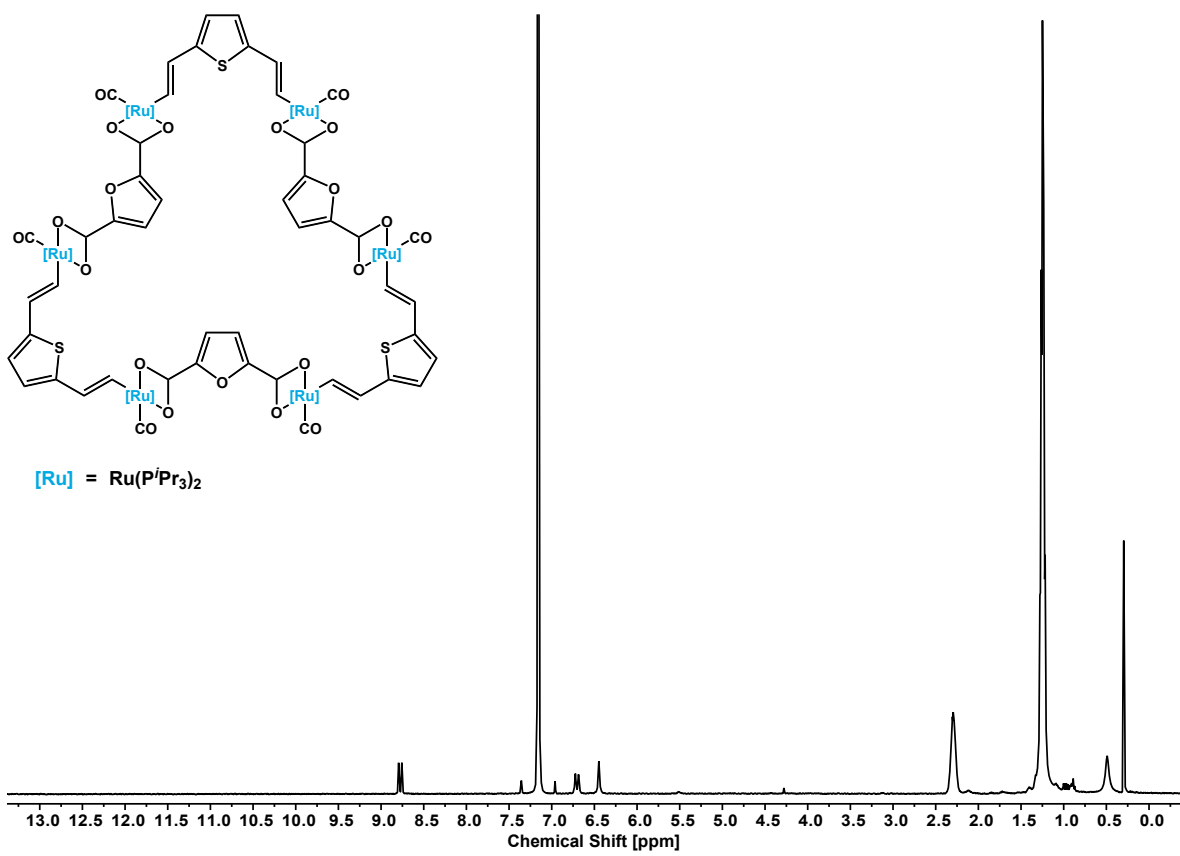


**Figure S3.** <sup>1</sup>H NMR spectrum of macrocycle **2-TF<sub>6</sub>**, measured in  $\text{C}_6\text{D}_6$ .

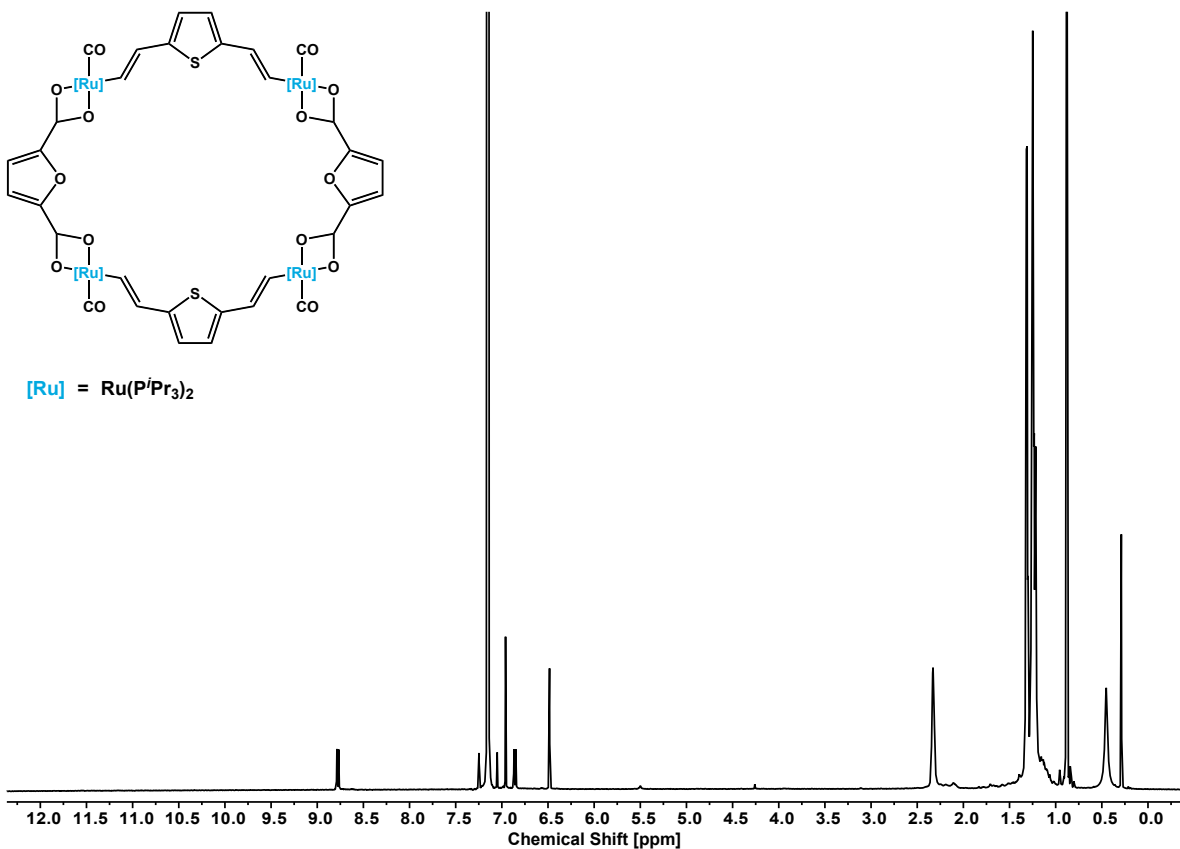


**Figure S4.** <sup>1</sup>H NMR spectrum of macrocycle **2-TF<sub>4</sub>**, measured in  $\text{C}_6\text{D}_6$ .

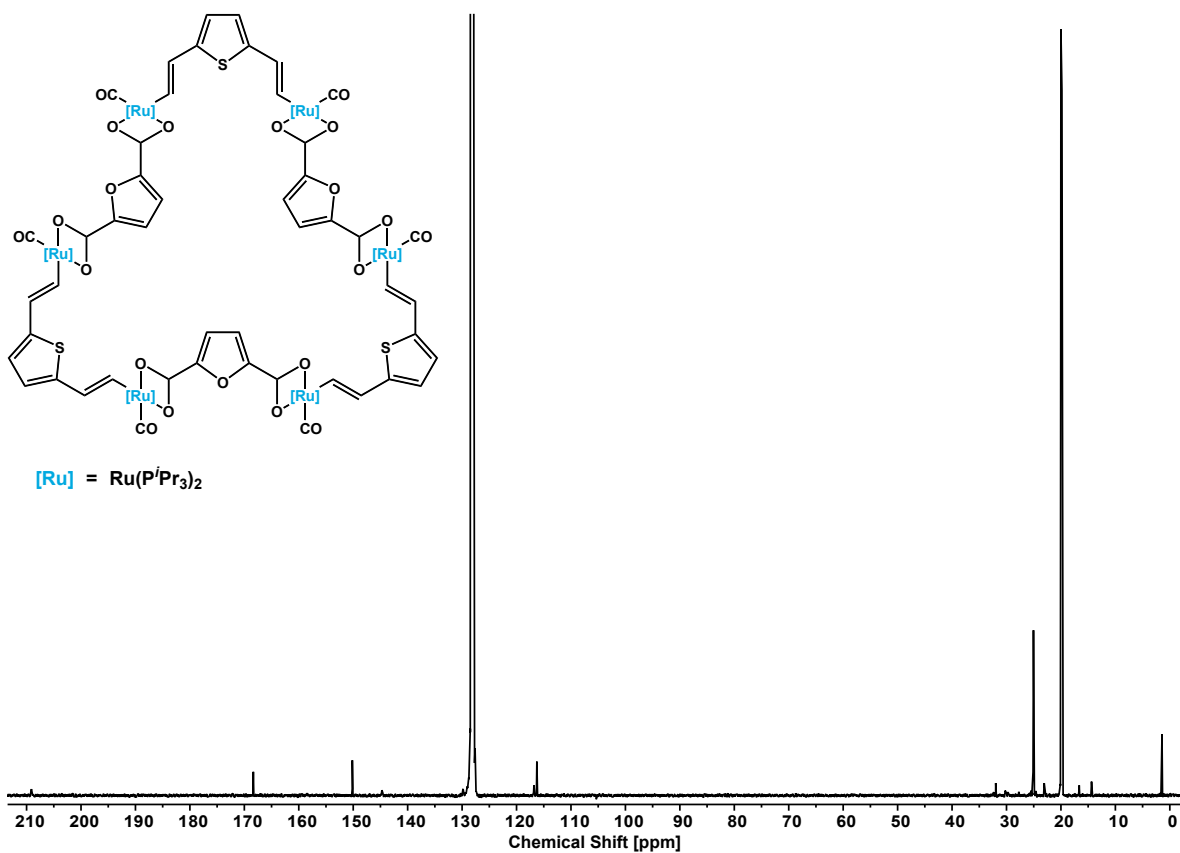


**Figure S5.**  $^{13}\text{C}\{^1\text{H}\}$  NMR spectrum of macrocycle **2-TF<sub>6</sub>**, measured in C<sub>6</sub>D<sub>6</sub>.

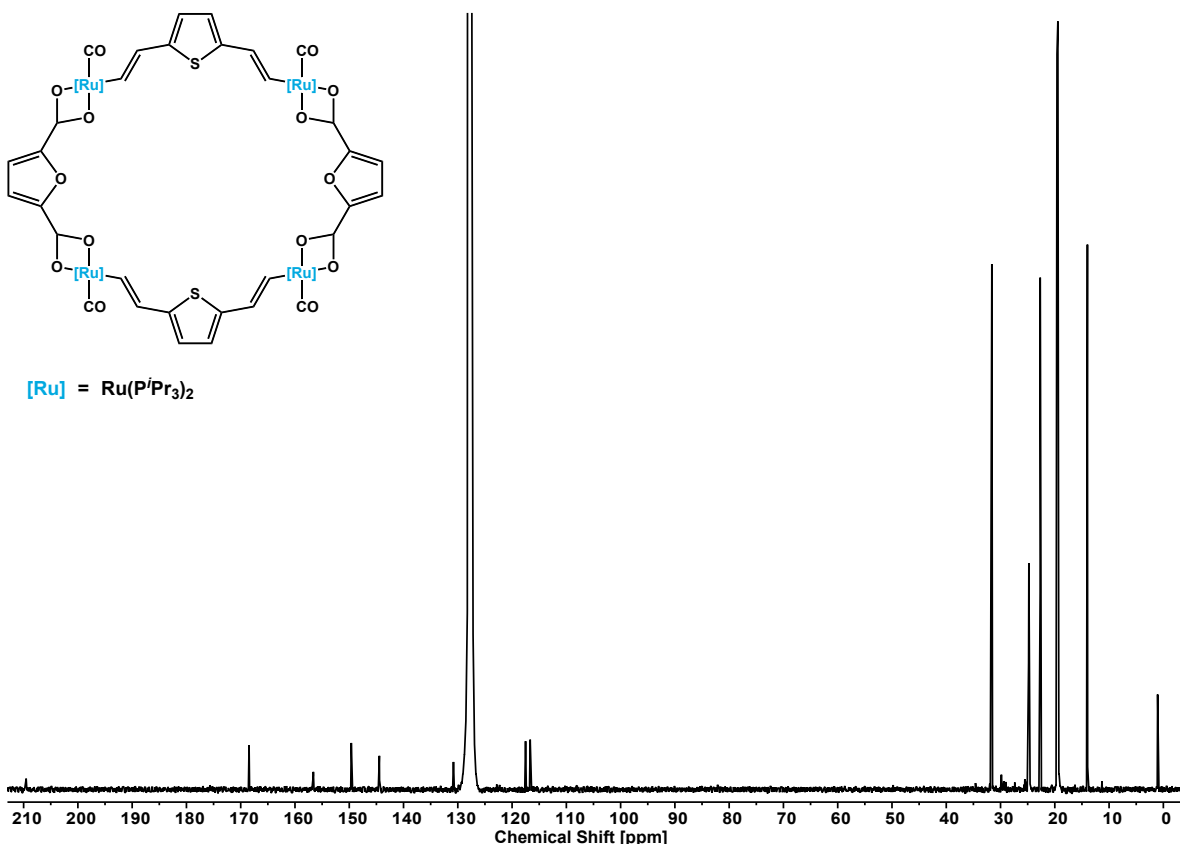


**Figure S6.**  $^{13}\text{C}\{^1\text{H}\}$  NMR spectrum of macrocycle **2-TF<sub>4</sub>**, measured in C<sub>6</sub>D<sub>6</sub>.

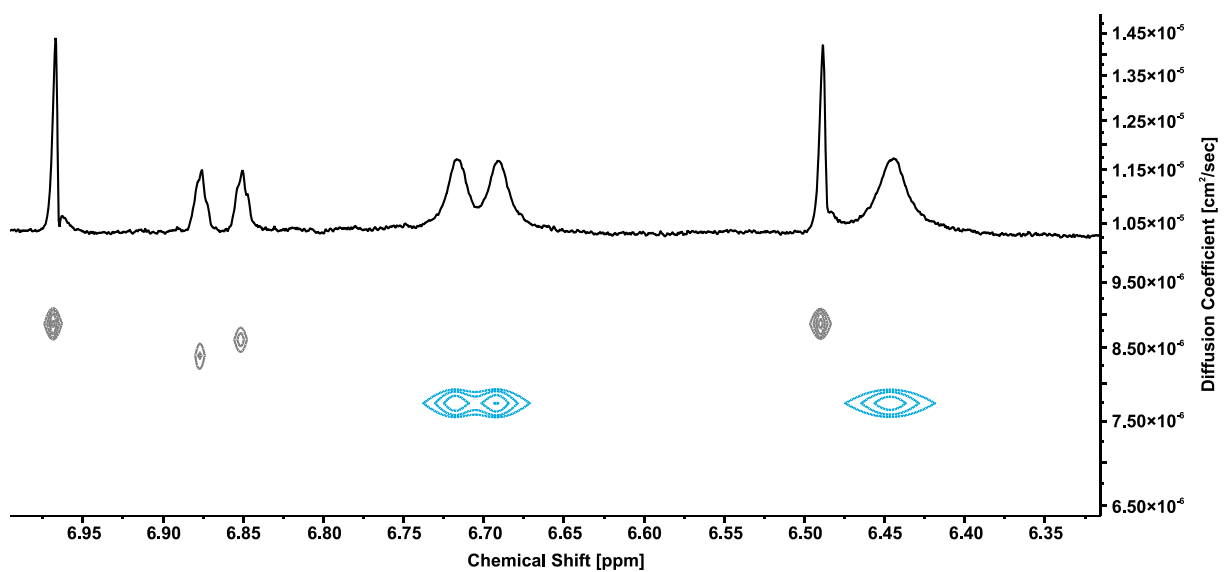


**Figure S7.** Excerpt from the DOSY spectrum of a mixture of the two macrocyclic isomers **2-TF<sub>4</sub>** (grey) and **2-TF<sub>6</sub>** (blue).

ESI MS

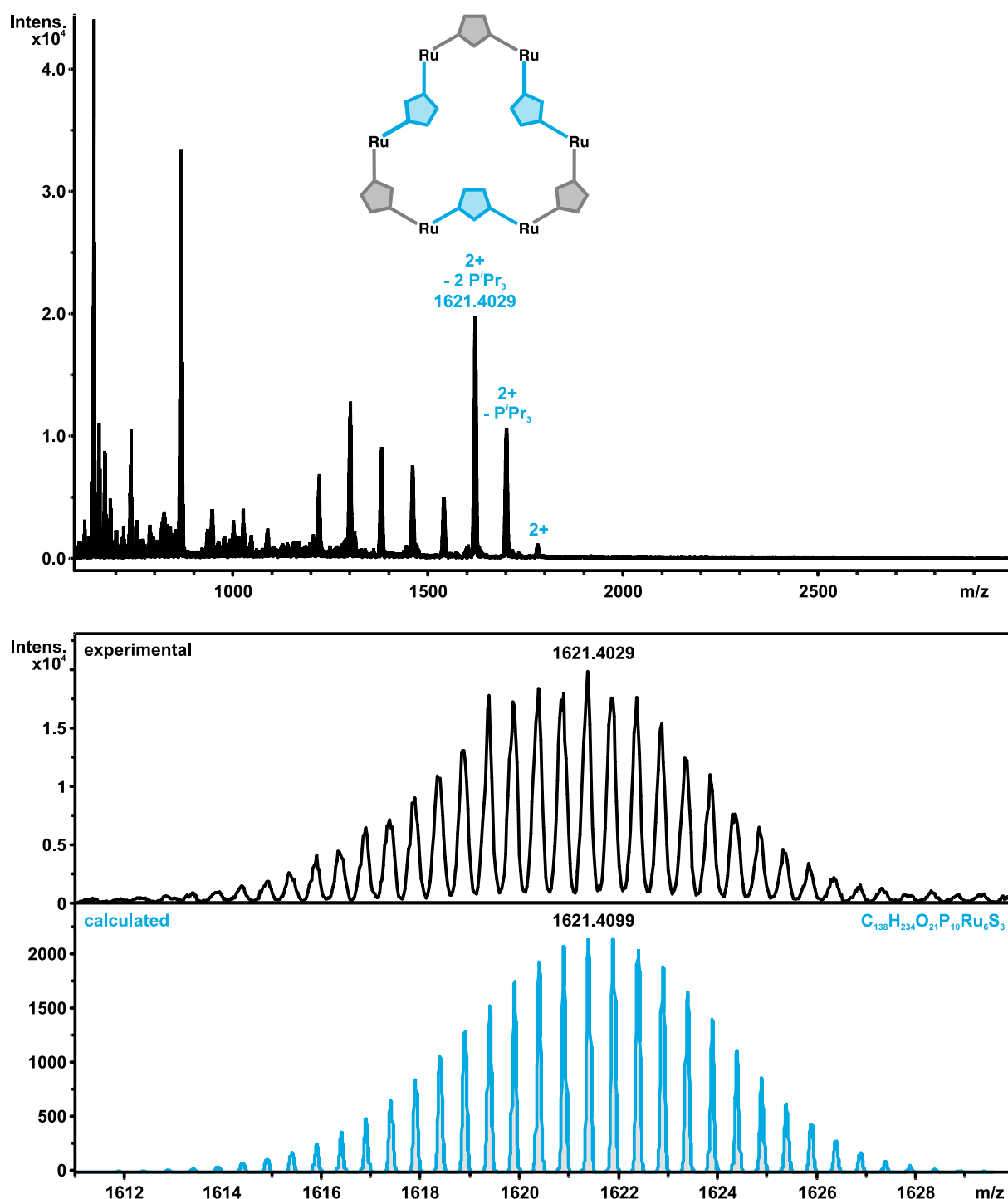


**Figure S8.** ESI Mass spectrum of macrocycle **2-TF<sub>6</sub>** (top), magnified  $[M - 2 P^iPr_3]^{2+}$  peak with calculated isotopic pattern (bottom).

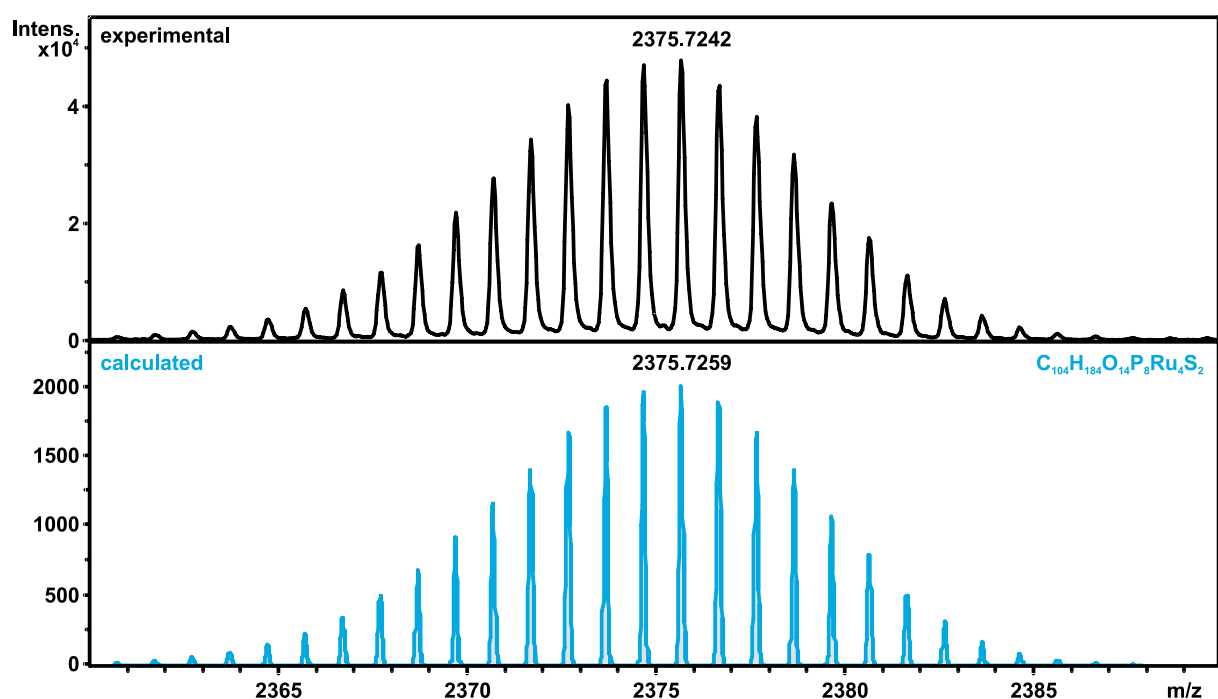
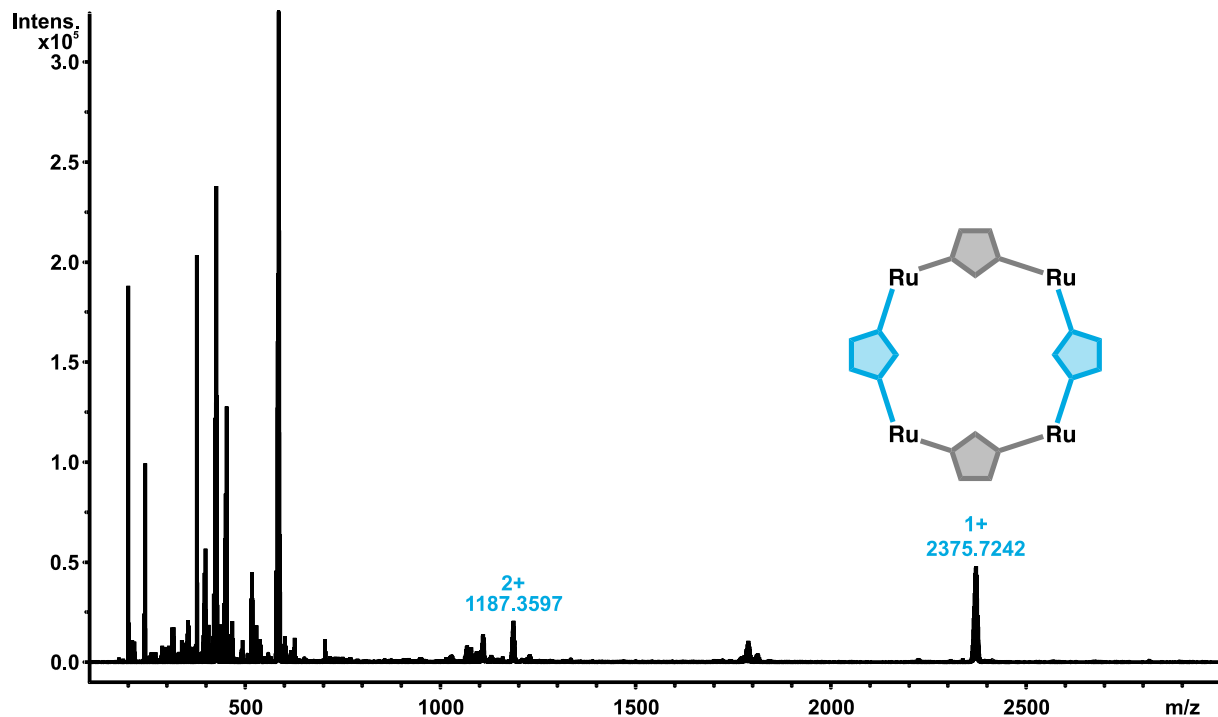


**Figure S9.** ESI Mass spectrum of macrocycle **2-TF<sub>4</sub>** (top), magnified M<sup>+</sup> peak with calculated isotopic pattern (bottom).

## X-ray Crystallography

### Compound 2-TF<sub>6</sub>:

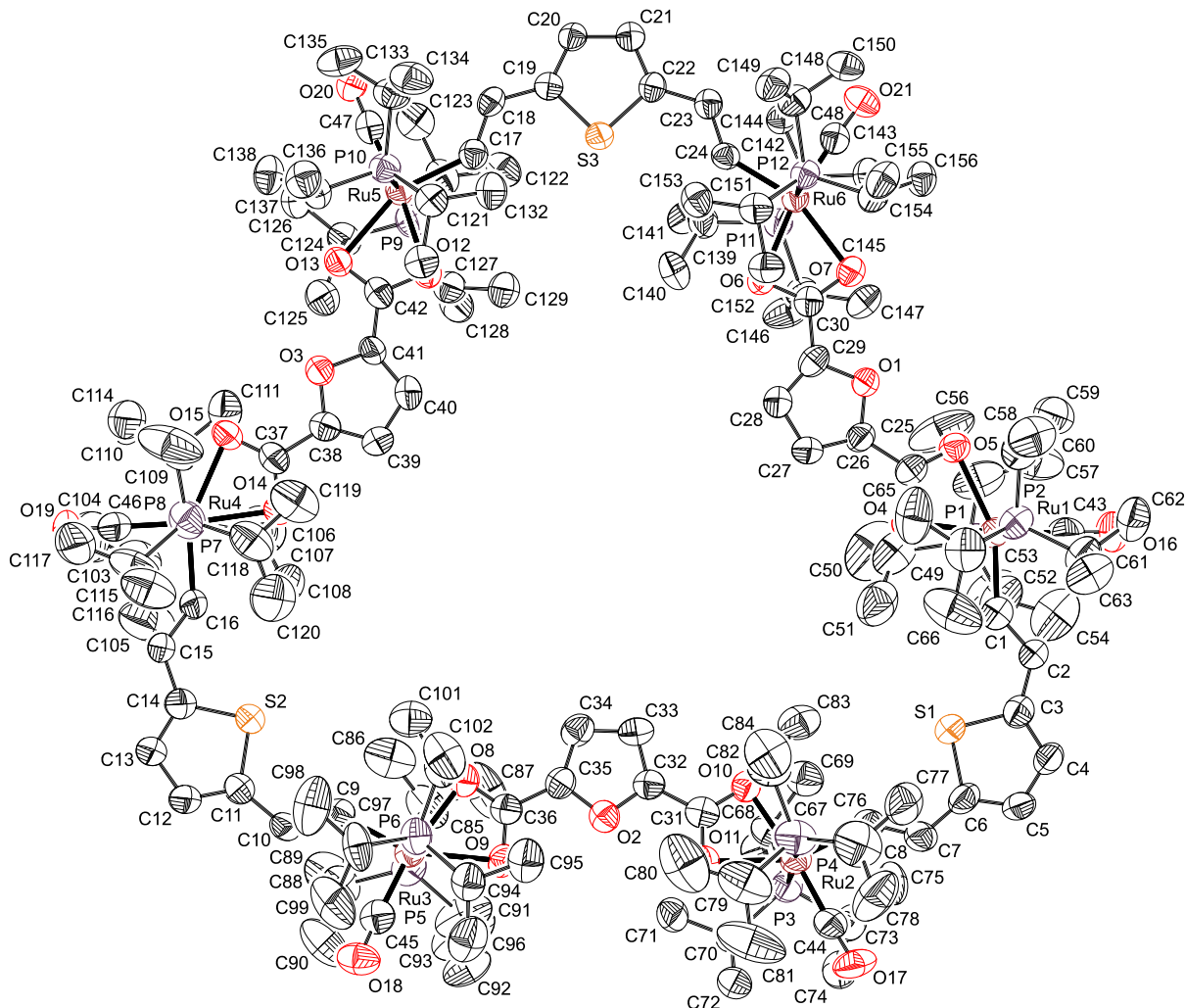


**Figure S10.** Structure of macrocycle **2-TF<sub>6</sub>** as the benzene dodecasolvate with atom numbering. Benzene solvate molecules as well as hydrogen atoms have been removed for reasons of clarity. Ellipsoids are drawn at a 50% probability level.

**Experimental.** Single crystals of **2-TF<sub>6</sub>** were obtained as yellow prisms by slow diffusion of methanol into a solution of compound **2-TF<sub>6</sub>** in benzene. A suitable crystal was selected, sealed in a Mark tube and mounted on a STOE IPDS-II diffractometer. The crystal was kept at 100.15 K during data collection. Using **Olex2<sup>(3)</sup>**, the structure was solved with the **ShelXT<sup>(5)</sup>** structure solution program using Intrinsic Phasing and refined with the **ShelXL<sup>(6)</sup>** refinement package using Least Squares minimization.

**Table S1.** Crystal data and structure refinement for macrocycle **2**- $\text{TF}_6\cdot\mathbf{12}\text{C}_6\text{H}_6$ .

Empirical formula	$\text{C}_{192}\text{H}_{312}\text{O}_{21}\text{P}_{12}\text{Ru}_6\text{S}_3$	
Formula weight	4030.64	
Temperature	100(3) K	
Wavelength	0.71073 Å	
Crystal system	Triclinic	
Space group	$P -1$	
Unit cell dimensions	$a = 23.3486(4)$ Å	$\alpha = 63.0890(10)$ °
	$b = 24.9671(5)$ Å	$\beta = 83.8960(10)$ °
	$c = 25.2132(5)$ Å	$\gamma = 71.9420(10)$ °
Volume	12450.7(4) Å <sup>3</sup>	
Z	2	
Density (calculated)	1.075 g/m <sup>3</sup>	
Absorption coefficient	0.505 mm <sup>-1</sup>	
$F(000)$	4248.0	
Crystal size	0.4 × 0.2 × 0.1 mm <sup>3</sup>	
2Θ range for data collection	4.6 to 52.5 °	
Index ranges	$-29 \leq h \leq 25, -31 \leq k \leq 31, -31 \leq l \leq 31$	
Reflections collected	92182	
Independent reflections	49773 [ $R_{\text{int}} = 0.0704, R_{\text{sigma}} = 0.0942$ ]	
Refinement method	Full-matrix least-squares on $F^2$	
Data / restraints / parameters	49773/208/2121	
Goodness-of-fit on $F^2$	1.050	
Final $R$ indices [ $I \geq 2\sigma(I)$ ]	$R_1 = 0.0848, wR_2 = 0.2212$	
$R$ indices (all data)	$R_1 = 0.1399, wR_2 = 0.2541$	
Largest diff. peak and hole	1.86 and -01.08 e Å <sup>-3</sup>	

**Table S2.** Selected bond lengths [Å] for **2-TF<sub>6</sub>·12 C<sub>6</sub>H<sub>6</sub>**.

Ru(1) - P(1)	2.435(2)	O(7) - C(30)	1.266(8)
Ru(1) - P(2)	2.380(2)	O(8) - C(36)	1.265(8)
Ru(1) - O(4)	2.214(5)	O(9) - C(36)	1.267(8)
Ru(1) - O(5)	2.290(5)	O(10) - C(31)	1.259(9)
Ru(1) - C(1)	1.982(8)	O(11) - C(31)	1.246(8)
Ru(1) - C(43)	1.788(10)	O(12) - C(42)	1.279(8)
Ru(2) - P(3)	2.393(2)	O(13) - C(42)	1.280(8)
Ru(2) - P(4)	2.399(2)	O(14) - C(37)	1.273(9)
Ru(2) - O(10)	2.199(5)	O(15) - C(37)	1.270(9)
Ru(2) - O(11)	2.275(5)	O(16) - C(43)	1.172(10)
Ru(2) - C(8)	2.015(8)	O(17) - C(44)	1.155(9)
Ru(2) - C(44)	1.814(8)	O(18) - C(45)	1.144(9)
Ru(3) - P(5)	2.413(2)	O(19) - C(46)	1.170(10)
Ru(3) - P(6)	2.415(2)	O(20) - C(47)	1.175(9)
Ru(3) - O(8)	2.209(5)	O(21) - C(48)	1.161(8)
Ru(3) - O(9)	2.267(5)	C(1) - C(2)	1.342(10)
Ru(3) - C(9)	1.976(7)	C(2) - C(3)	1.457(11)
Ru(3) - C(45)	1.795(9)	C(3) - C(4)	1.357(10)
Ru(4) - P(7)	2.388(2)	C(4) - C(5)	1.390(11)
Ru(4) - P(8)	2.370(3)	C(5) - C(6)	1.361(11)
Ru(4) - O(14)	2.209(5)	C(6) - C(7)	1.438(12)
Ru(4) - O(15)	2.341(5)	C(7) - C(8)	1.307(11)
Ru(4) - C(16)	1.990(7)	C(9) - C(10)	1.352(10)
Ru(4) - C(46)	1.813(10)	C(10) - C(11)	1.452(10)
Ru(5) - P(9)	2.425(2)	C(11) - C(12)	1.350(12)
Ru(5) - P(10)	2.3956(19)	C(12) - C(13)	1.436(12)
Ru(5) - O(12)	2.198(5)	C(13) - C(14)	1.364(12)
Ru(5) - O(13)	2.307(5)	C(14) - C(15)	1.447(11)
Ru(5) - C(17)	2.005(7)	C(15) - C(16)	1.321(10)
Ru(5) - C(47)	1.779(8)	C(17) - C(18)	1.357(10)
Ru(6) - P(11)	2.4479(17)	C(18) - C(19)	1.453(9)
Ru(6) - P(12)	2.3913(17)	C(19) - C(20)	1.346(9)

Ru(6) - O(6)	2.222(5)	C(20) - C(21)	1.413(9)
Ru(6) - O(7)	2.267(4)	C(21) - C(22)	1.361(9)
Ru(6) - C(24)	1.992(6)	C(22) - C(23)	1.428(9)
Ru(6) - C(48)	1.808(8)	C(23) - C(24)	1.358(9)
S(1) - C(3)	1.754(8)	C(25) - C(26)	1.481(10)
S(1) - C(6)	1.733(8)	C(26) - C(27)	1.351(11)
S(2) - C(11)	1.727(8)	C(27) - C(28)	1.380(11)
S(2) - C(14)	1.737(9)	C(28) - C(29)	1.338(11)
S(3) - C(19)	1.752(6)	C(29) - C(30)	1.459(10)
S(3) - C(22)	1.756(7)	C(31) - C(32)	1.484(10)
O(1) - C(26)	1.353(8)	C(32) - C(33)	1.362(10)
O(1) - C(29)	1.368(8)	C(33) - C(34)	1.430(11)
O(2) - C(32)	1.372(8)	C(34) - C(35)	1.363(11)
O(2) - C(35)	1.340(9)	C(35) - C(36)	1.468(10)
O(3) - C(38)	1.375(8)	C(37) - C(38)	1.468(10)
O(3) - C(41)	1.376(8)	C(38) - C(39)	1.331(10)
O(4) - C(25)	1.288(9)	C(39) - C(40)	1.400(11)
O(5) - C(25)	1.220(9)	C(40) - C(41)	1.358(10)
O(6) - C(30)	1.267(8)	C(41) - C(42)	1.420(10)

**Table S3.** Selected bond angles [°] for **2-TF<sub>6</sub>·12 C<sub>6</sub>H<sub>6</sub>**.

O(4) - Ru(1) - O(5)	58.36(18)	O(6) - Ru(6) - P(11)	85.67(12)
O(4) - Ru(1) - P(1)	87.95(15)	O(6) - Ru(6) - P(12)	92.47(12)
O(4) - Ru(1) - P(2)	89.67(14)	O(7) - Ru(6) - P(11)	93.48(12)
O(5) - Ru(1) - P(1)	90.09(13)	O(7) - Ru(6) - P(12)	88.64(12)
O(5) - Ru(1) - P(2)	88.14(13)	P(11) - Ru(6) - P(12)	175.92(7)
P(1) - Ru(1) - P(2)	177.54(8)	C(24) - Ru(6) - O(6)	98.8(2)
C(1) - Ru(1) - O(4)	96.7(3)	C(24) - Ru(6) - O(7)	157.2(2)
C(1) - Ru(1) - O(5)	155.0(3)	C(24) - Ru(6) - P(11)	86.59(18)
C(1) - Ru(1) - P(1)	91.1(2)	C(24) - Ru(6) - P(12)	90.11(18)
C(1) - Ru(1) - P(2)	89.8(2)	C(48) - Ru(6) - O(6)	169.2(3)
C(43) - Ru(1) - O(4)	173.4(3)	C(48) - Ru(6) - O(7)	111.1(3)
C(43) - Ru(1) - O(5)	115.2(3)	C(48) - Ru(6) - P(11)	92.4(2)
C(43) - Ru(1) - P(1)	91.1(3)	C(48) - Ru(6) - P(12)	90.1(2)
C(43) - Ru(1) - P(2)	91.2(3)	C(48) - Ru(6) - C(24)	91.7(3)
C(43) - Ru(1) - C(1)	89.8(4)	O(21) - C(48) - Ru(6)	177.3(7)
O(16) - C(43) - Ru(1)	177.5(9)	C(23) - C(24) - Ru(6)	138.8(5)
C(2) - C(1) - Ru(1)	140.0(7)	C(30) - O(6) - Ru(6)	91.4(4)
C(25) - O(4) - Ru(1)	90.6(4)	C(30) - O(7) - Ru(6)	89.4(4)
C(25) - O(5) - Ru(1)	88.8(4)	C(1) - C(2) - C(3)	123.9(8)
O(10) - Ru(2) - O(11)	58.53(18)	C(2) - C(3) - S(1)	119.6(6)
O(10) - Ru(2) - P(3)	88.87(13)	C(3) - C(4) - C(5)	115.2(8)
O(10) - Ru(2) - P(4)	90.77(14)	C(4) - C(3) - S(1)	107.9(6)
O(11) - Ru(2) - P(3)	87.74(14)	C(4) - C(3) - C(2)	132.5(8)
O(11) - Ru(2) - P(4)	86.95(14)	C(5) - C(6) - S(1)	108.6(7)
P(3) - Ru(2) - P(4)	173.99(9)	C(5) - C(6) - C(7)	131.5(7)
C(8) - Ru(2) - O(10)	95.8(3)	C(6) - C(5) - C(4)	114.9(7)
C(8) - Ru(2) - O(11)	154.4(2)	C(6) - S(1) - C(3)	93.5(4)
C(8) - Ru(2) - P(3)	92.2(2)	C(7) - C(6) - S(1)	119.8(6)
C(8) - Ru(2) - P(4)	93.9(2)	C(8) - C(7) - C(6)	125.0(7)
C(44) - Ru(2) - O(10)	174.3(3)	C(9) - C(10) - C(11)	126.4(7)
C(44) - Ru(2) - O(11)	115.9(3)	C(10) - C(11) - S(2)	121.2(6)
C(44) - Ru(2) - P(3)	89.8(2)	C(11) - C(12) - C(13)	113.5(8)

C(44) - Ru(2) - P(4)	90.0(2)	C(12) - C(11) - S(2)	110.2(6)
C(44) - Ru(2) - C(8)	89.8(3)	C(12) - C(11) - C(10)	128.6(8)
O(17) - C(44) - Ru(2)	176.2(8)	C(13) - C(14) - S(2)	109.3(6)
C(7) - C(8) - Ru(2)	139.8(6)	C(13) - C(14) - C(15)	129.7(8)
C(31) - O(10) - Ru(2)	91.4(4)	C(14) - C(13) - C(12)	113.6(8)
C(31) - O(11) - Ru(2)	88.3(5)	C(14) - S(2) - C(11)	93.4(4)
O(8) - Ru(3) - O(9)	58.81(19)	C(15) - C(14) - S(2)	121.1(6)
O(8) - Ru(3) - P(5)	91.02(13)	C(16) - C(15) - C(14)	124.6(7)
O(8) - Ru(3) - P(6)	87.17(13)	C(17) - C(18) - C(19)	123.4(6)
O(9) - Ru(3) - P(5)	89.64(14)	C(18) - C(19) - S(3)	120.8(5)
O(9) - Ru(3) - P(6)	87.41(14)	C(19) - C(20) - C(21)	115.3(6)
P(5) - Ru(3) - P(6)	177.03(8)	C(20) - C(19) - S(3)	109.0(5)
C(9) - Ru(3) - O(8)	97.9(3)	C(20) - C(19) - C(18)	130.2(6)
C(9) - Ru(3) - O(9)	156.7(3)	C(21) - C(22) - S(3)	109.0(5)
C(9) - Ru(3) - P(5)	89.8(2)	C(21) - C(22) - C(23)	130.6(7)
C(9) - Ru(3) - P(6)	92.8(2)	C(22) - C(21) - C(20)	113.9(6)
C(45) - Ru(3) - O(8)	169.3(3)	C(22) - S(3) - C(19)	92.8(3)
C(45) - Ru(3) - O(9)	110.8(3)	C(23) - C(22) - S(3)	120.3(5)
C(45) - Ru(3) - P(5)	91.8(2)	C(24) - C(23) - C(22)	125.2(7)
C(45) - Ru(3) - P(6)	89.5(2)	O(4) - C(25) - O(5)	122.2(7)
C(45) - Ru(3) - C(9)	92.5(4)	O(4) - C(25) - C(26)	116.6(7)
O(18) - C(45) - Ru(3)	177.6(8)	O(5) - C(25) - C(26)	121.1(7)
C(10) - C(9) - Ru(3)	137.7(6)	C(25) - C(26) - O(1)	116.7(6)
C(36) - O(8) - Ru(3)	91.6(4)	C(25) - C(26) - C(27)	134.1(7)
C(36) - O(9) - Ru(3)	88.9(4)	C(26) - O(1) - C(29)	106.6(6)
O(14) - Ru(4) - O(15)	58.13(18)	C(26) - C(27) - C(28)	107.5(7)
O(14) - Ru(4) - P(7)	88.40(15)	C(27) - C(26) - O(1)	109.2(6)
O(14) - Ru(4) - P(8)	91.21(15)	C(27) - C(28) - C(29)	107.2(7)
O(15) - Ru(4) - P(7)	88.44(15)	C(28) - C(29) - O(1)	109.5(6)
O(15) - Ru(4) - P(8)	88.82(15)	C(28) - C(29) - C(30)	133.9(7)
P(7) - Ru(4) - P(8)	176.98(9)	O(1) - C(29) - C(30)	116.6(7)
C(16) - Ru(4) - O(14)	94.9(3)	O(6) - C(30) - C(29)	118.9(6)
C(16) - Ru(4) - O(15)	152.9(3)	O(7) - C(30) - O(6)	120.1(6)

C(16) - Ru(4) - P(7)	93.4(2)	O(7) - C(30) - C(29)	120.9(6)
C(16) - Ru(4) - P(8)	89.6(2)	O(10) - C(31) - O(11)	121.8(7)
C(46) - Ru(4) - O(14)	174.0(3)	O(10) - C(31) - C(32)	118.9(7)
C(46) - Ru(4) - O(15)	116.6(3)	O(11) - C(31) - C(32)	119.3(7)
C(46) - Ru(4) - P(7)	88.6(3)	C(31) - C(32) - O(2)	116.2(6)
C(46) - Ru(4) - P(8)	91.5(3)	C(31) - C(32) - C(33)	132.4(8)
C(46) - Ru(4) - C(16)	90.5(3)	C(32) - O(2) - C(35)	106.5(6)
O(19) - C(46) - Ru(4)	178.7(10)	C(32) - C(33) - C(34)	105.9(7)
C(15) - C(16) - Ru(4)	140.1(6)	C(33) - C(32) - O(2)	111.4(7)
C(37) - O(14) - Ru(4)	93.4(4)	C(33) - C(34) - C(35)	105.7(7)
C(37) - O(15) - Ru(4)	87.5(4)	C(34) - C(35) - O(2)	110.4(7)
O(12) - Ru(5) - O(13)	58.69(17)	C(34) - C(35) - C(36)	132.8(7)
O(12) - Ru(5) - P(9)	86.65(13)	O(2) - C(35) - C(36)	116.8(7)
O(12) - Ru(5) - P(10)	89.51(12)	O(9) - C(36) - C(35)	119.7(7)
O(13) - Ru(5) - P(9)	86.61(12)	O(8) - C(36) - O(9)	120.5(7)
O(13) - Ru(5) - P(10)	88.26(12)	O(8) - C(36) - C(35)	119.7(7)
P(9) - Ru(5) - P(10)	174.69(7)	O(14) - C(37) - O(15)	121.0(7)
C(17) - Ru(5) - O(12)	96.9(2)	O(14) - C(37) - C(38)	116.9(7)
C(17) - Ru(5) - O(13)	155.5(2)	O(15) - C(37) - C(38)	122.1(7)
C(17) - Ru(5) - P(9)	92.94(19)	C(37) - C(38) - O(3)	116.4(6)
C(17) - Ru(5) - P(10)	91.16(19)	C(37) - C(38) - C(39)	132.6(7)
C(47) - Ru(5) - O(12)	173.6(3)	C(38) - O(3) - C(41)	105.6(5)
C(47) - Ru(5) - O(13)	115.0(3)	C(38) - C(39) - C(40)	106.8(7)
C(47) - Ru(5) - P(9)	92.1(2)	C(39) - C(38) - O(3)	111.0(7)
C(47) - Ru(5) - P(10)	91.3(2)	C(39) - C(40) - C(41)	107.4(7)
C(47) - Ru(5) - C(17)	89.5(3)	C(40) - C(41) - O(3)	109.2(6)
O(20) - C(47) - Ru(5)	177.1(7)	C(40) - C(41) - C(42)	133.1(7)
C(18) - C(17) - Ru(5)	134.6(5)	O(3) - C(41) - C(42)	117.5(6)
C(42) - O(12) - Ru(5)	93.3(4)	O(13) - C(42) - C(41)	121.8(6)
C(42) - O(13) - Ru(5)	88.4(4)	O(12) - C(42) - O(13)	119.4(6)
O(6) - Ru(6) - O(7)	58.55(17)	O(12) - C(42) - C(41)	118.7(7)

**Compound 2-TF<sub>4</sub>:**

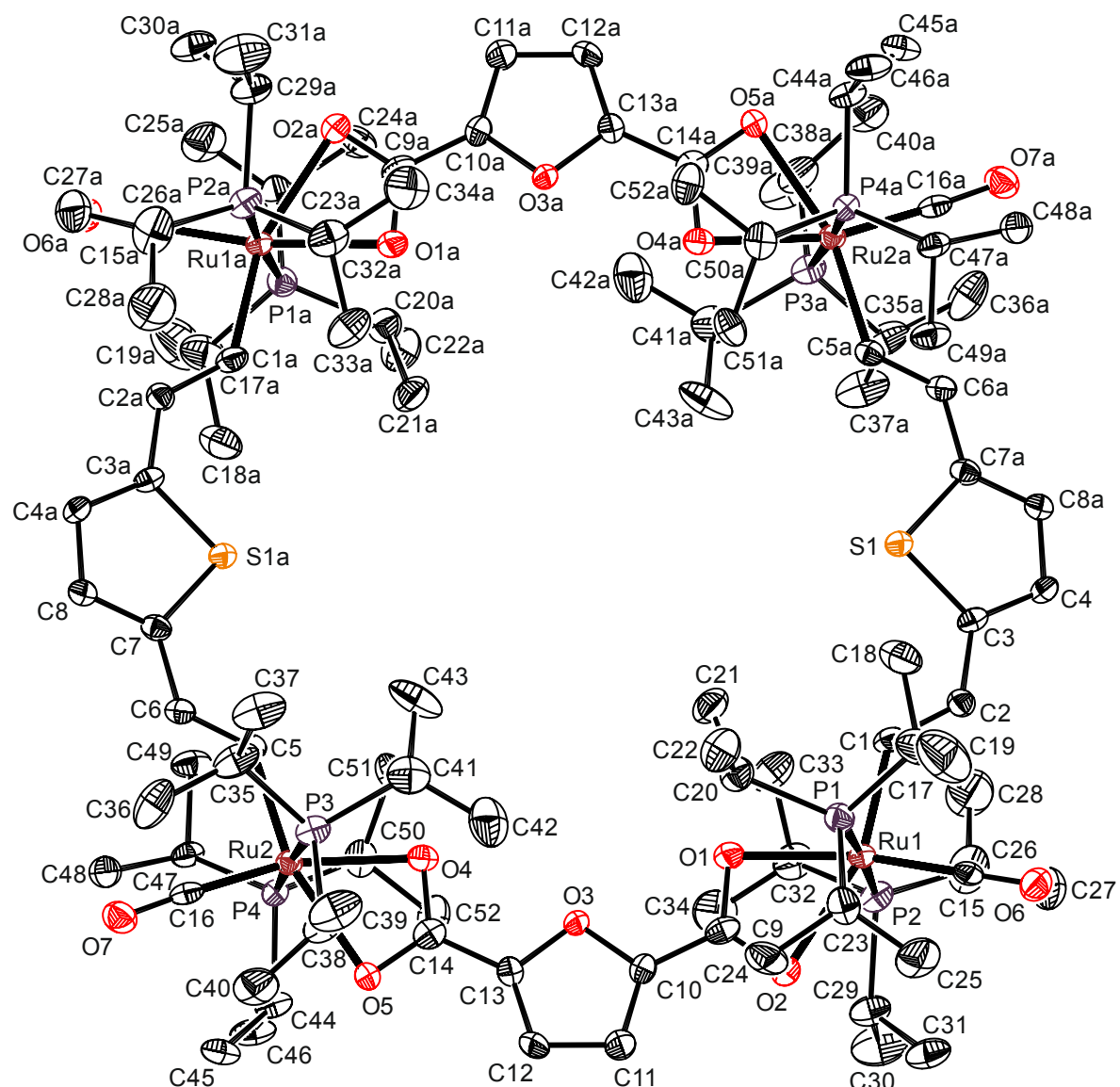


**Figure S11.** Structure of macrocycle **2-TF<sub>4</sub>** as the benzene tetrasolvate with atom numbering. Benzene solvate molecules as well as hydrogen atoms have been removed for clarity reasons. Ellipsoids are drawn at a 50% probability level.

**Experimental.** Single crystals of **2-TF<sub>4</sub>** were obtained as yellow prisms by slow diffusion of methanol into a solution of compound **2-TF<sub>4</sub>** in benzene. A suitable crystal was selected and mounted on a STOE IPDS-II diffractometer. The crystal was kept at 100.15 K during data collection. Using **Olex2<sup>(3)</sup>**, the structure was solved with the **SIR2004<sup>(4)</sup>** structure solution program using Direct Methods and refined with the **ShelXL<sup>(6)</sup>** refinement package using Least Squares minimization.

**Table S4.** Crystal data and structure refinement for macrocycle **2**-TF<sub>4</sub>·4 C<sub>6</sub>H<sub>6</sub>.

Empirical formula	C <sub>134</sub> H <sub>214</sub> O <sub>14</sub> P <sub>8</sub> Ru <sub>4</sub> S <sub>2</sub>	
Formula weight	2765.20	
Temperature	100.15 K	
Wavelength	0.71073 Å	
Crystal system	Triclinic	
Space group	<i>P</i> -1	
Unit cell dimensions	<i>a</i> = 11.9389(9) Å	$\alpha$ = 102.732(6) °
	<i>b</i> = 17.3830(15) Å	$\beta$ = 98.198(6) °
	<i>c</i> = 18.6230(15) Å	$\gamma$ = 101.465(6) °
Volume	3623.7(5) Å <sup>3</sup>	
<i>Z</i>	1	
Density (calculated)	1.267 g/m <sup>3</sup>	
Absorption coefficient	0.580 mm <sup>-1</sup>	
<i>F</i> (000)	1458.0	
Crystal size	0.4 × 0.3 × 0.2 mm <sup>3</sup>	
2Θ range for data collection	3.548 to 53.716 °	
Index ranges	-15 ≤ <i>h</i> ≤ 15, -22 ≤ <i>k</i> ≤ 22, -23 ≤ <i>l</i> ≤ 23	
Reflections collected	52347	
Independent reflections	15420 [ <i>R</i> <sub>int</sub> = 0.1519, <i>R</i> <sub>sigma</sub> = 0.1730]	
Refinement method	Full-matrix least-squares on F <sup>2</sup>	
Data / restraints / parameters	15420/8/754	
Goodness-of-fit on <i>F</i> <sup>2</sup>	0.866	
Final <i>R</i> indices [I ≥ 2σ (I)]	<i>R</i> <sub>1</sub> = 0.0595, w <i>R</i> <sub>2</sub> = 0.0787	
<i>R</i> indices (all data)	<i>R</i> <sub>1</sub> = 0.1321, w <i>R</i> <sub>2</sub> = 0.0926	
Largest diff. peak and hole	0.85 and -0.62 e Å <sup>-3</sup>	

**Table S5.** Selected bond lengths [Å] for **2-TF<sub>4</sub>·4 C<sub>6</sub>H<sub>6</sub>**.

Ru(1) - P(1)	2.4102(16)	O(4) - C(14)	1.282(5)
Ru(1) - P(2)	2.4196(17)	O(5) - C(14)	1.257(5)
Ru(1) - O(1)	2.202(3)	O(6) - C(15)	1.162(6)
Ru(1) - O(2)	2.289(3)	O(7) - C(16)	1.185(6)
Ru(1) - C(1)	2.013(4)	S(1) - C(3)	1.740(5)
Ru(1) - C(9)	2.594(5)	S(1) - C(7a)	1.759(5)
Ru(1) - C(15)	1.805(5)	C(1) - C(2)	1.349(6)
Ru(2) - P(3)	2.4138(16)	C(2) - C(3)	1.451(6)
Ru(2) - P(4)	2.3840(16)	C(3) - C(4)	1.378(7)
Ru(2) - O(4)	2.211(3)	C(4) - C(8a)	1.417(6)
Ru(2) - O(5)	2.276(3)	C(5) - C(6)	1.320(7)
Ru(2) - C(5)	2.020(5)	C(6) - C(7)	1.453(6)
Ru(2) - C(14)	2.583(5)	C(7) - C(8)	1.352(7)
Ru(2) - C(16)	1.784(5)	C(9) - C(10)	1.459(7)
O(1) - C(9)	1.272(5)	C(10) - C(11)	1.366(6)
O(2) - C(9)	1.266(6)	C(11) - C(12)	1.409(7)
O(3) - C(10)	1.355(5)	C(12) - C(13)	1.342(6)
O(3) - C(13)	1.372(5)	C(13) - C(14)	1.464(7)

**Table S6.** Selected bond angles [°] for **2-TF<sub>4</sub>·4 C<sub>6</sub>H<sub>6</sub>**.

O(1) - Ru(1) - O(2)	58.52(11)	C(16) - Ru(2) - C(5)	90.3(2)
O(1) - Ru(1) - P(1)	88.19(10)	C(9) - O(1) - Ru(1)	92.7(3)
O(1) - Ru(1) - P(2)	88.54(10)	C(9) - O(2) - Ru(1)	88.9(3)
O(1) - Ru(1) - C(9)	29.32(13)	C(10) - O(3) - C(13)	106.0(3)
O(2) - Ru(1) - P(1)	89.82(10)	C(14) - O(4) - Ru(2)	91.4(3)
O(2) - Ru(1) - P(2)	87.60(10)	C(14) - O(5) - Ru(2)	89.1(3)
O(2) - Ru(1) - C(9)	29.22(13)	C(3) - S(1) - C(7a)	92.4(2)
P(1) - Ru(1) - P(2)	176.57(5)	C(2) - C(1) - Ru(1)	132.0(4)
P(1) - Ru(1) - C(9)	88.10(12)	C(1) - C(2) - C(3)	126.9(5)
P(2) - Ru(1) - C(9)	88.55(12)	C(2) - C(3) - S(1)	125.2(4)
C(1) - Ru(1) - O(1)	100.85(17)	C(4) - C(3) - S(1)	110.1(3)
C(1) - Ru(1) - O(2)	159.29(16)	C(4) - C(3) - C(2)	124.7(4)
C(1) - Ru(1) - P(1)	91.38(15)	C(3) - C(4) - C(8a)	113.1(4)
C(1) - Ru(1) - P(2)	90.24(15)	C(10) - C(11) - C(12)	106.0(4)
C(1) - Ru(1) - C(9)	130.17(18)	O(3) - C(10) - C(11)	110.5(4)
C(15) - Ru(1) - O(1)	169.75(16)	O(3) - C(10) - C(9)	117.4(4)
C(15) - Ru(1) - O(2)	111.55(16)	C(11) - C(10) - C(9)	132.1(4)
C(15) - Ru(1) - P(1)	89.26(17)	O(1) - C(9) - Ru(1)	58.0(2)
C(15) - Ru(1) - P(2)	93.79(18)	O(1) - C(9) - C(10)	121.2(4)
C(15) - Ru(1) - C(1)	89.1(2)	O(2) - C(9) - Ru(1)	61.9(3)
C(15) - Ru(1) - C(9)	140.65(17)	O(2) - C(9) - O(1)	119.9(5)
O(4) - Ru(2) - O(5)	58.83(11)	O(2) - C(9) - C(10)	118.9(4)
O(4) - Ru(2) - P(3)	87.55(9)	C(10) - C(9) - Ru(1)	174.8(4)
O(4) - Ru(2) - P(4)	88.61(9)	C(13) - C(12) - C(11)	106.9(4)
O(4) - Ru(2) - C(14)	29.75(12)	O(3) - C(13) - C(14)	117.1(4)
O(5) - Ru(2) - P(3)	88.82(9)	C(12) - C(13) - O(3)	110.6(4)
O(5) - Ru(2) - P(4)	89.76(9)	C(12) - C(13) - C(14)	132.1(4)
O(5) - Ru(2) - C(14)	29.11(12)	O(4) - C(14) - Ru(2)	58.8(2)
P(3) - Ru(2) - C(14)	86.92(11)	O(4) - C(14) - C(13)	120.4(4)
P(4) - Ru(2) - P(3)	176.10(5)	O(5) - C(14) - Ru(2)	61.8(2)
P(4) - Ru(2) - C(14)	90.08(11)	O(5) - C(14) - O(4)	120.5(4)
C(5) - Ru(2) - O(4)	104.52(16)	O(5) - C(14) - C(13)	119.1(4)

C(5) - Ru(2) - O(5)	163.34(15)	C(13) - C(14) - Ru(2)	175.6(4)
C(5) - Ru(2) - P(3)	89.84(14)	O(6) - C(15) - Ru(1)	178.0(5)
C(5) - Ru(2) - P(4)	90.48(14)	C(6) - C(5) - Ru(2)	131.9(4)
C(5) - Ru(2) - C(14)	134.23(17)	C(5) - C(6) - C(7)	129.5(4)
C(16) - Ru(2) - O(4)	165.18(16)	C(6) - C(7) - S(1a)	122.8(4)
C(16) - Ru(2) - O(5)	106.35(16)	C(8) - C(7) - S(1a)	109.6(3)
C(16) - Ru(2) - P(3)	92.71(17)	C(8) - C(7) - C(6)	127.6(4)
C(16) - Ru(2) - P(4)	91.18(17)	C(7) - C(8) - C(4a)	114.8(4)
C(16) - Ru(2) - C(14)	135.45(18)	O(7) - C(16) - Ru(2)	177.1(4)

## Cyclic Voltammetry

**Compound 2-TF<sub>6</sub>:**

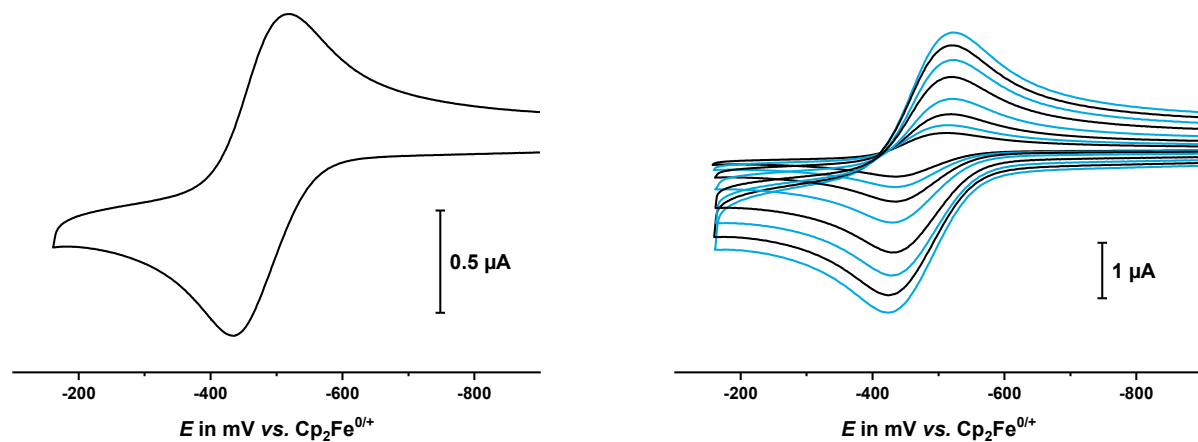


**Figure S12.** Cyclic voltammograms for the first composite wave of macrocycle **2-TF<sub>6</sub>** at  $v = 100$  mV/s (left) and at  $v = 25, 50, 100, 200, 400, 600, 800, 1000$  mV/s (right) in  $\text{CH}_2\text{Cl}_2/n\text{Bu}_4\text{NBAr}^{\text{F24}}$ .

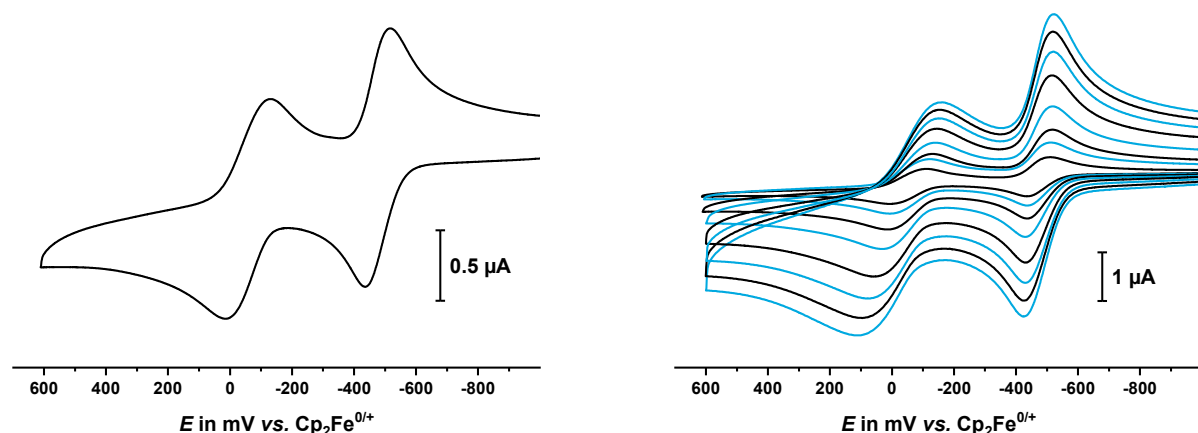


**Figure S13.** Cyclic voltammograms for the first two composite waves of macrocycle **2-TF<sub>6</sub>** at  $v = 100$  mV/s (left) and at  $v = 25, 50, 100, 200, 400, 600, 800, 1000$  mV/s (right) in  $\text{CH}_2\text{Cl}_2/n\text{Bu}_4\text{NBAr}^{\text{F24}}$ .

**Table S7.** Data of the cyclovoltammetric measurements for macrocycle **2-TF<sub>6</sub>** at different scan rates, measured in CH<sub>2</sub>Cl<sub>2</sub>/nBu<sub>4</sub>NBAr<sup>F24</sup>.

$v$ in mV/s	$E_{1/2}^{0/3+}$ in mV	$\Delta E_p^{0/3+}$ in mV	$E_{1/2}^{3+/6+}$ in mV	$\Delta E_p^{3+/6+}$ in mV	$\Delta E$ in mV
<b>25</b>	-474	78	-51	117	423
<b>50</b>	-474	80	-56	129	418
<b>100</b>	-476	84	-57	147	419
<b>200</b>	-475	91	-54	172	421
<b>400</b>	-475	91	-43	201	432
<b>600</b>	-475	93	-38	227	437
<b>800</b>	-472	98	-29	252	443
<b>1000</b>	-473	99	-22	274	451

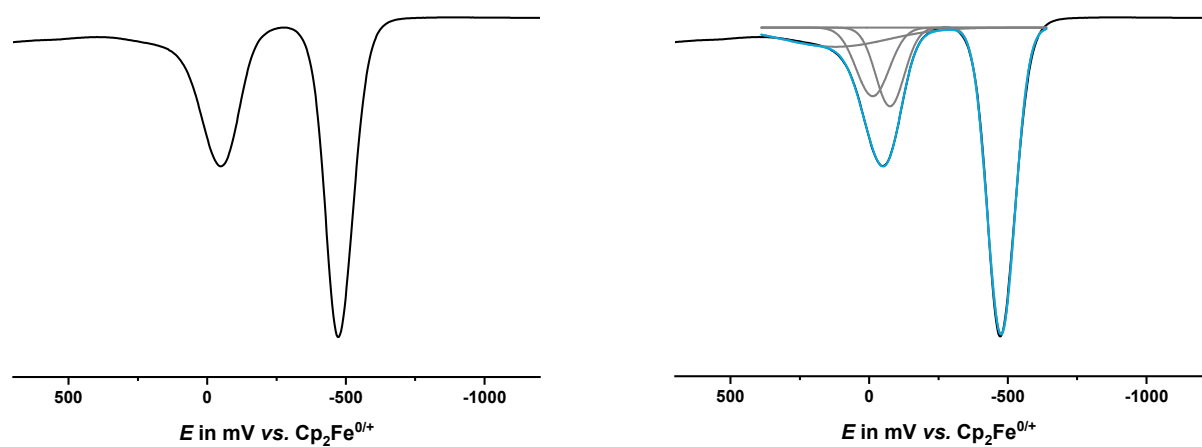


**Figure S14.** Square wave voltammogram of macrocycle **2-TF<sub>6</sub>** (left) with deconvolution (right), measured in CH<sub>2</sub>Cl<sub>2</sub>/nBu<sub>4</sub>NBAr<sup>F24</sup>.

**Compound 2-TF<sub>4</sub>:**

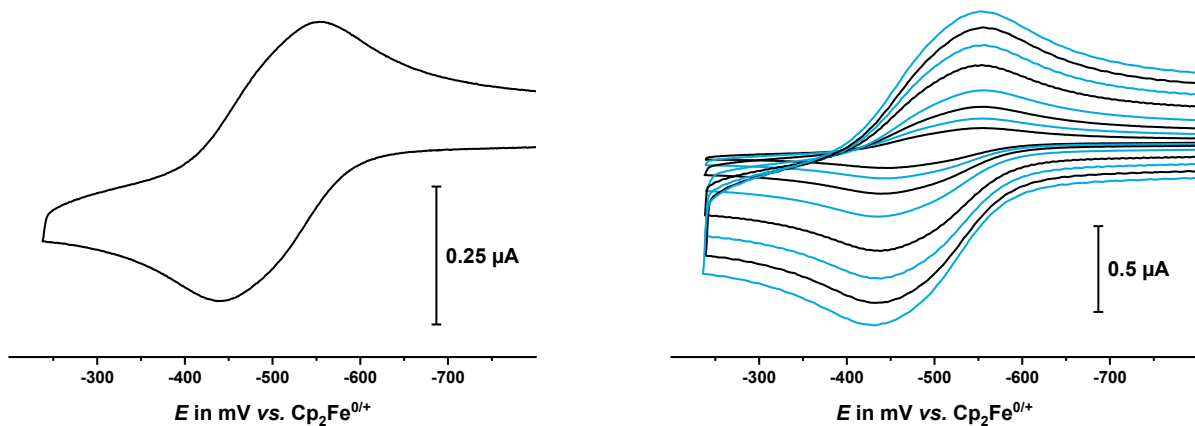


**Figure S15.** Cyclic voltammograms for the first composite wave of macrocycle **2-TF<sub>4</sub>** at  $v = 100$  mV/s (left) and at  $v = 25, 50, 100, 200, 400, 600, 800, 1000$  mV/s (right) in CH<sub>2</sub>Cl<sub>2</sub>/<sup>n</sup>Bu<sub>4</sub>NBAr<sup>F24</sup>.

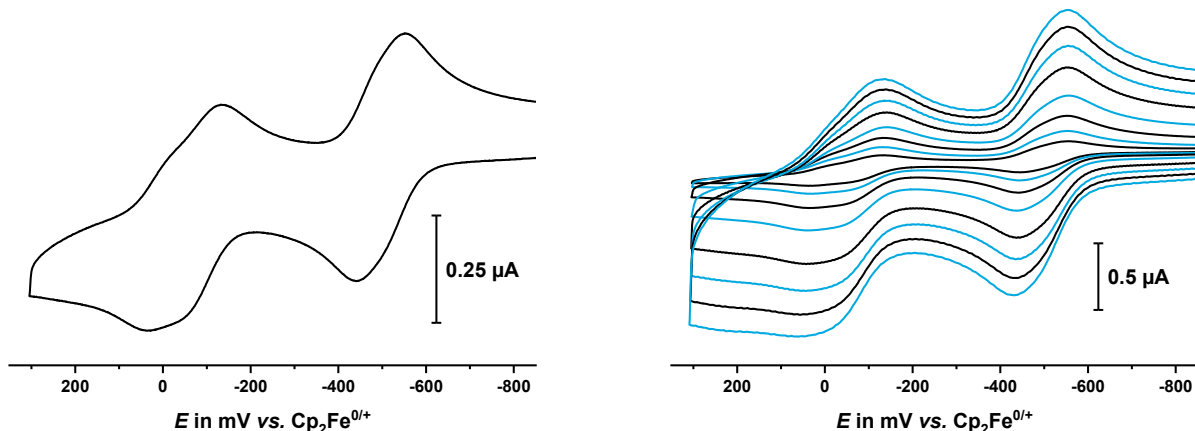


**Figure S16.** Cyclic voltammograms for the first two composite waves of macrocycle **2-TF<sub>4</sub>** at  $v = 100$  mV/s (left) and at  $v = 25, 50, 100, 200, 400, 600, 800, 1000$  mV/s (right) in CH<sub>2</sub>Cl<sub>2</sub>/<sup>n</sup>Bu<sub>4</sub>NBAr<sup>F24</sup>.

**Table S8.** Data of the cyclovoltammetric measurements for macrocycle **2-TF<sub>4</sub>** at different scan rates, measured in CH<sub>2</sub>Cl<sub>2</sub>/<sup>n</sup>Bu<sub>4</sub>NBAr<sup>F24</sup>.

$v$ in mV/s	$E_{1/2}^{0/2+}$ in mV	$\Delta E_p^{0/2+}$ in mV	$E_{1/2}^{2+/4+}$ in mV	$\Delta E_p^{2+/4+}$ in mV	$\Delta E$ in mV
<b>25</b>	-499	112	-48	168	451
<b>50</b>	-499	107	-49	162	450
<b>100</b>	-497	111	-49	170	447
<b>200</b>	-496	119	-51	180	445
<b>400</b>	-496	116	-49	184	446
<b>600</b>	-497	116	-48	183	449
<b>800</b>	-493	120	-42	193	452
<b>1000</b>	-492	123	-33	201	458

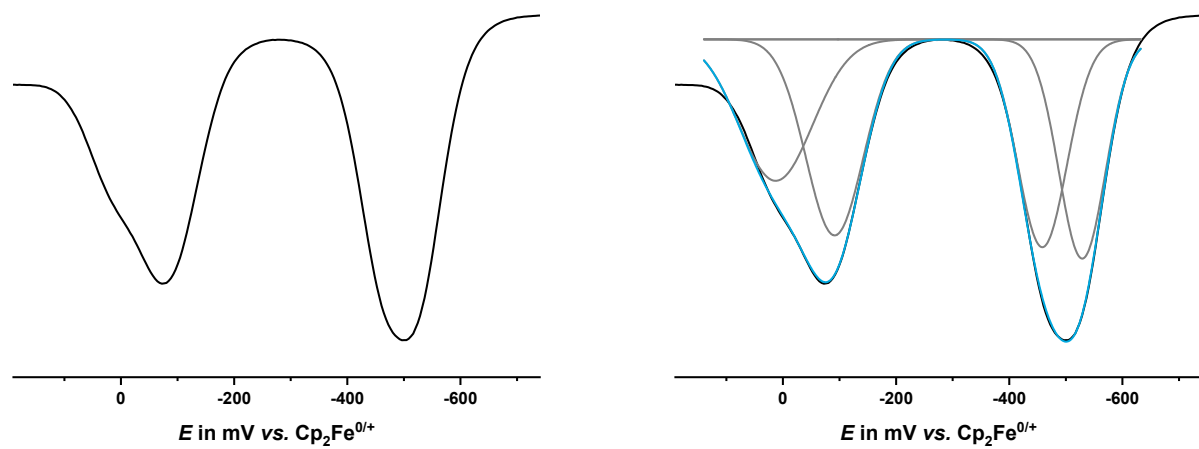


**Figure S17.** Square wave voltammogram of macrocycle **2-TF<sub>4</sub>** (left) with deconvolution (right), measured in CH<sub>2</sub>Cl<sub>2</sub>/<sup>n</sup>Bu<sub>4</sub>NBAr<sup>F24</sup>.

## Spectroelectrochemistry

**Compound 2-TF<sub>6</sub>:**

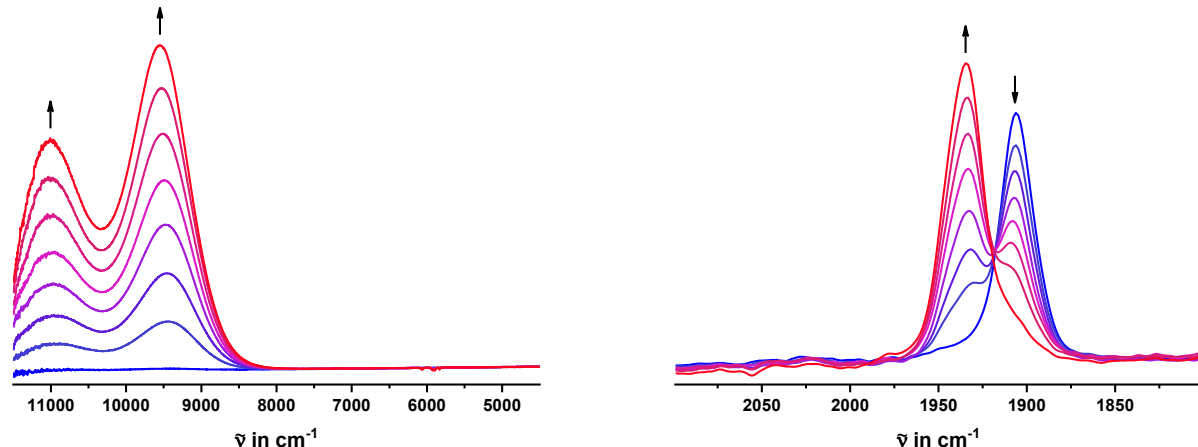


**Figure S18.** Changes in the NIR (left) and mid-IR (Ru(CO)) (right) spectra of  $\mathbf{2}\text{-TF}_6$  upon oxidation to  $\mathbf{2}\text{-TF}_6^{3+}$ , measured in  $\text{CH}_2\text{Cl}_2/\text{nBu}_4\text{NPF}_6$  (0.2 M, r. t.).

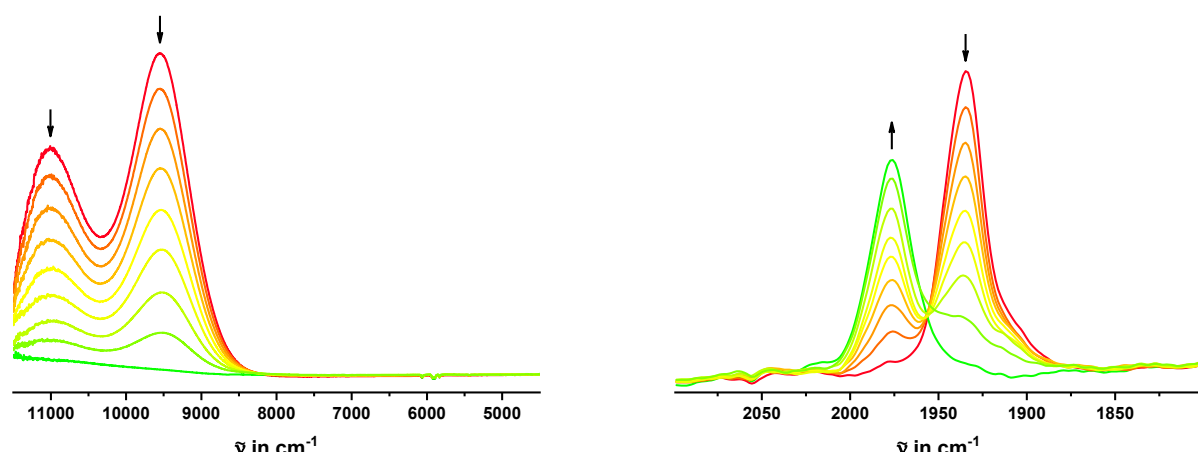


**Figure S19.** Changes in the NIR (left) and mid-IR (Ru(CO)) (right) spectra of  $\mathbf{2}\text{-TF}_6^{3+}$  upon further oxidation to  $\mathbf{2}\text{-TF}_6^{6+}$ , measured in  $\text{CH}_2\text{Cl}_2/\text{nBu}_4\text{NPF}_6$  (0.2 M, r. t.).

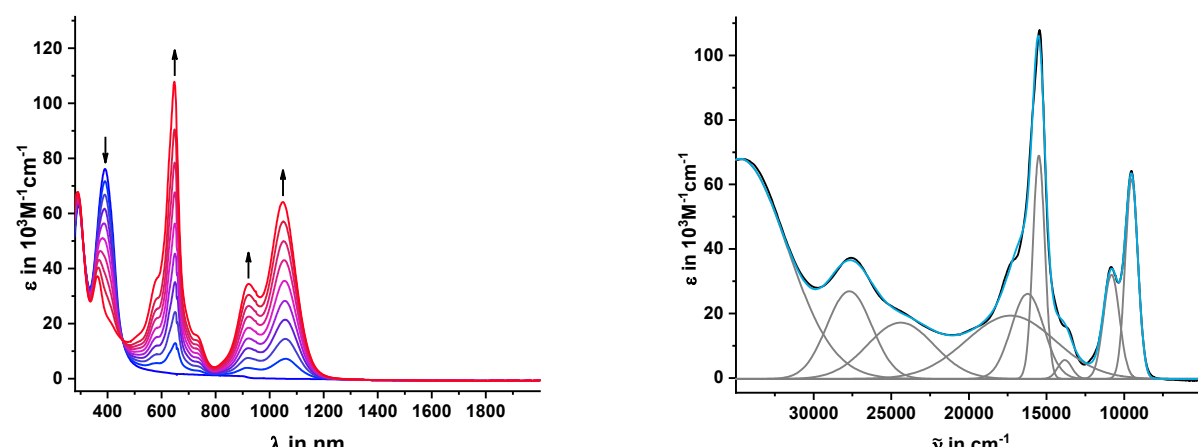


**Figure S20.** Changes in the UV/Vis/NIR spectra of  $\mathbf{2}\text{-TF}_6$  upon oxidation to  $\mathbf{2}\text{-TF}_6^{3+}$  (left) and deconvolution (right), measured in  $\text{CH}_2\text{Cl}_2/\text{nBu}_4\text{NPF}_6$  (0.2 M, r. t.).

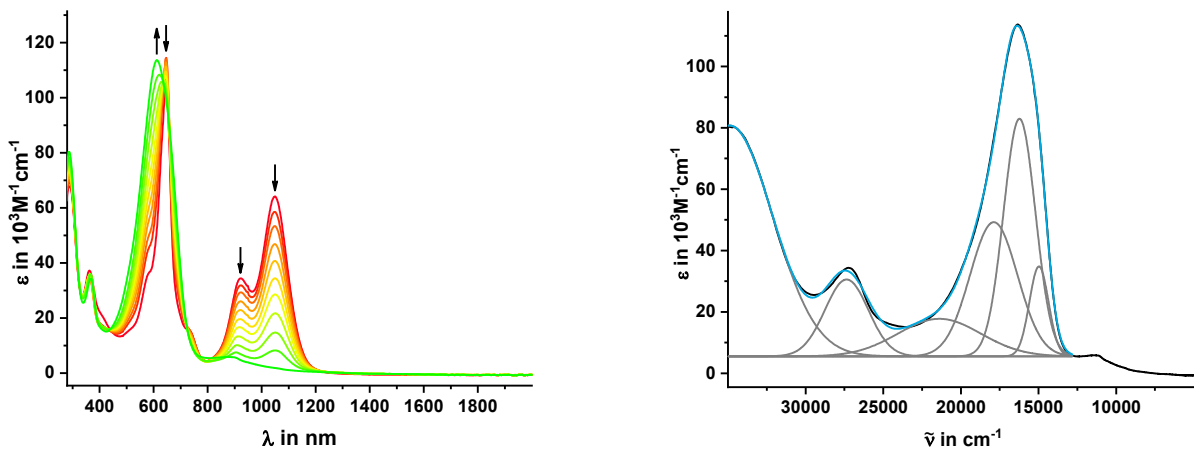


**Figure S21.** Changes in the UV/Vis/NIR spectra upon further oxidation of  $\mathbf{2}\text{-TF}_6^{3+}$  to  $\mathbf{2}\text{-TF}_6^{6+}$  (left) and deconvolution (right), measured in  $\text{CH}_2\text{Cl}_2/n\text{Bu}_4\text{NPF}_6$  (0.2 M, r. t.).

#### Compound $\mathbf{2}\text{-TF}_4$ :

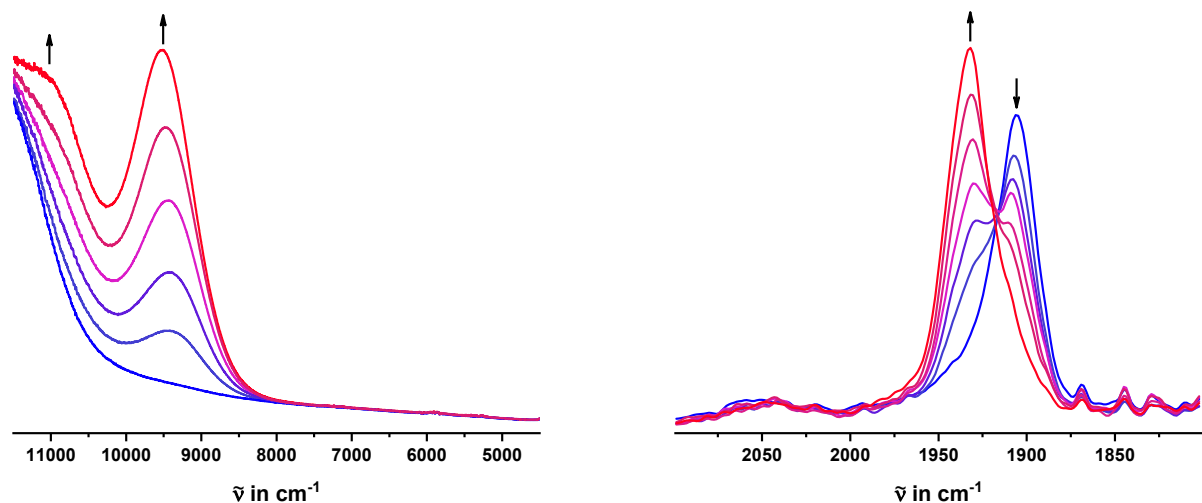


**Figure S22.** Changes in the NIR (left) and mid-IR (Ru(CO)) (right) spectra of  $\mathbf{2}\text{-TF}_4$  upon oxidation to  $\mathbf{2}\text{-TF}_4^{2+}$ , measured in  $\text{CH}_2\text{Cl}_2/n\text{Bu}_4\text{NPF}_6$  (0.2 M, r. t.).

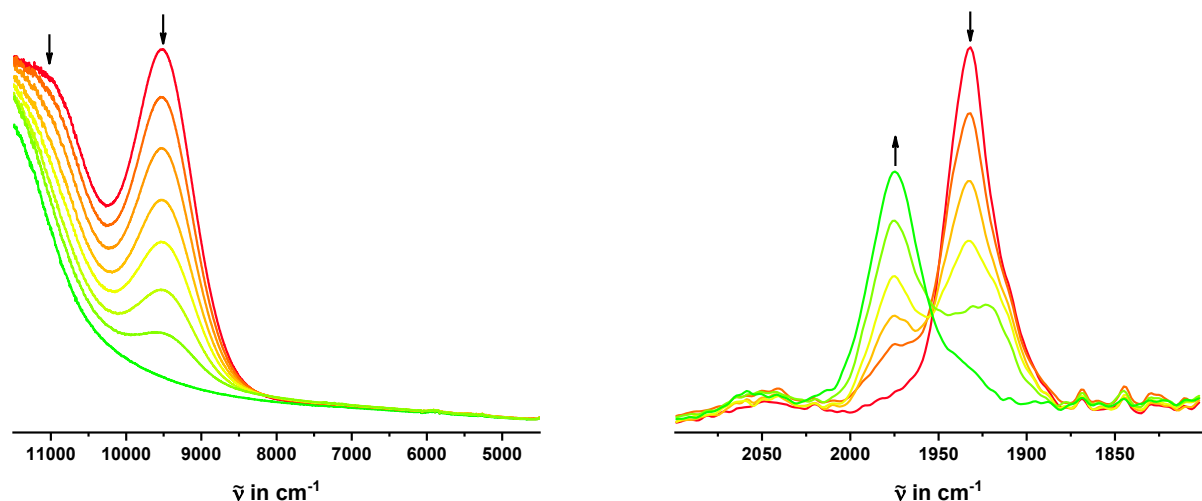


**Figure S23.** Changes in the NIR (left) and mid-IR (Ru(CO)) (right) spectra upon further oxidation of  $\mathbf{2}\text{-TF}_4^{2+}$  to  $\mathbf{2}\text{-TF}_4^{4+}$ , measured in  $\text{CH}_2\text{Cl}_2/n\text{Bu}_4\text{NPF}_6$  (0.2 M, r. t.).

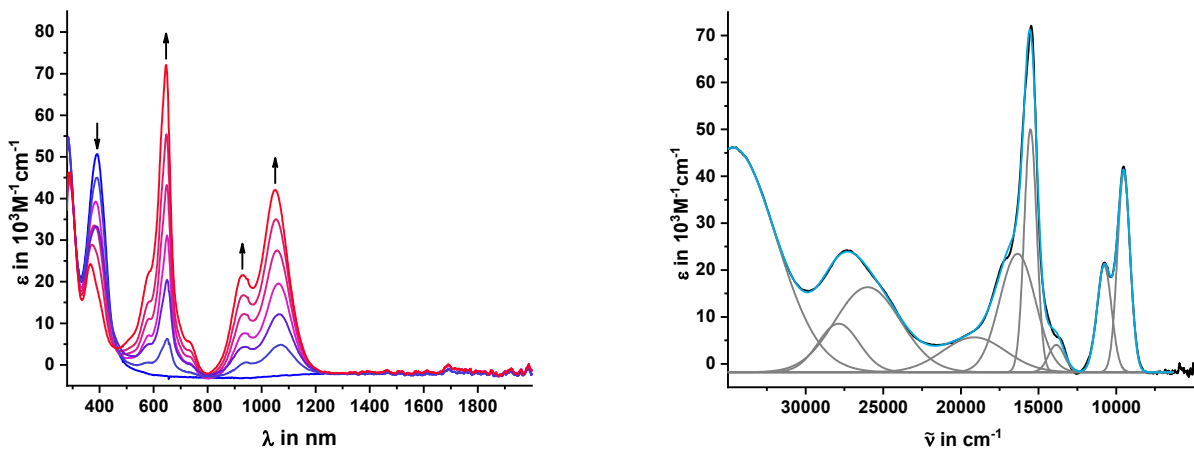


**Figure S24.** Changes in the UV/Vis/NIR spectra of **2**–TF<sub>4</sub> upon oxidation to **2**–TF<sub>4</sub><sup>2+</sup> (left) and deconvolution (right), measured in CH<sub>2</sub>Cl<sub>2</sub>/<sup>n</sup>Bu<sub>4</sub>NPF<sub>6</sub> (0.2 M, r. t.).

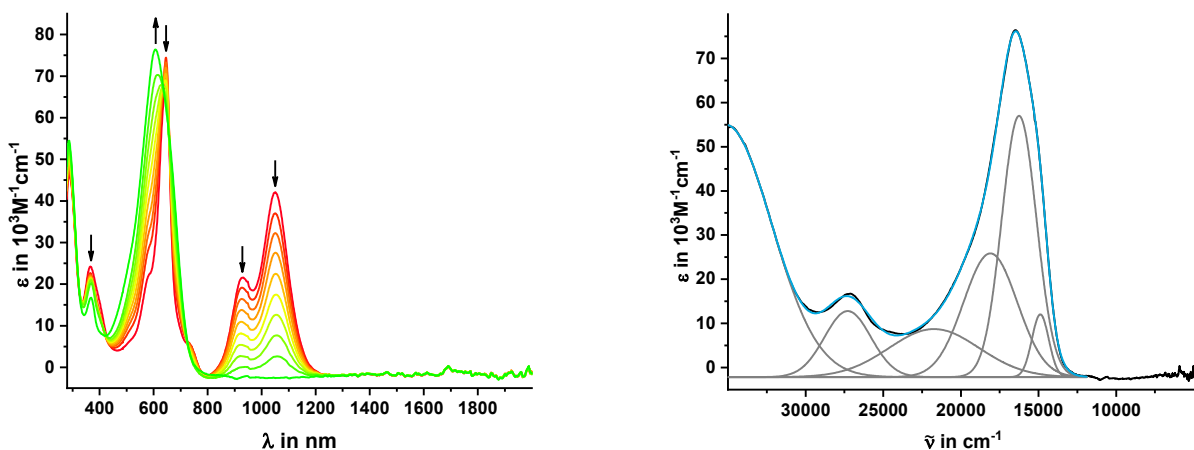


**Figure S25.** Changes in the UV/Vis/NIR spectra upon further oxidation of **2**–TF<sub>4</sub><sup>2+</sup> to **2**–TF<sub>4</sub><sup>4+</sup> (left) and deconvolution (right), measured in CH<sub>2</sub>Cl<sub>2</sub>/<sup>n</sup>Bu<sub>4</sub>NPF<sub>6</sub> (0.2 M, r. t.).

## EPR Spectroscopy

Compound 2-TF<sub>6</sub>:

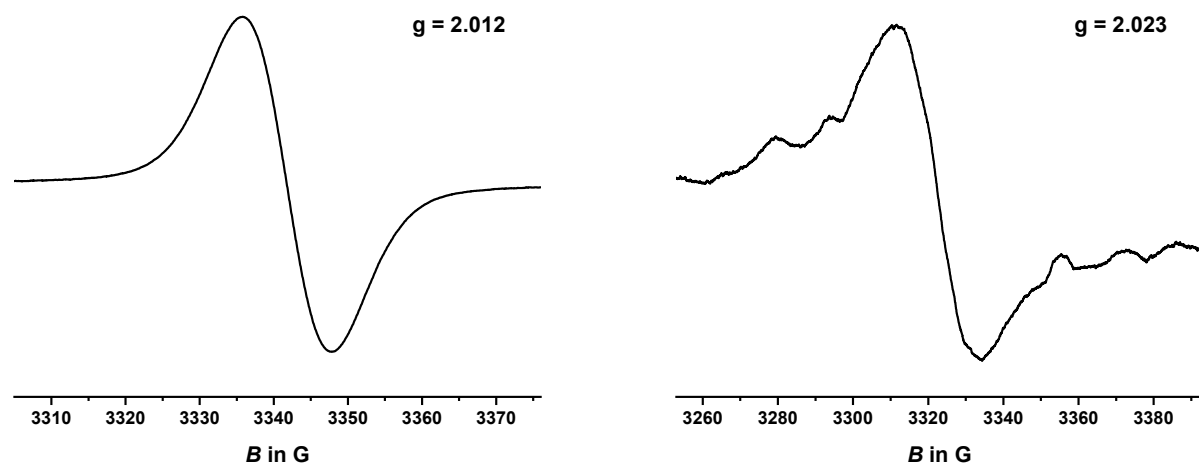


Figure S26. EPR spectra of  $\mathbf{2}\text{-TF}_6^{3+}$  (left) and  $\mathbf{2}\text{-TF}_6^{6+}$  (right) at room temperature.

Compound 2-TF<sub>4</sub>:

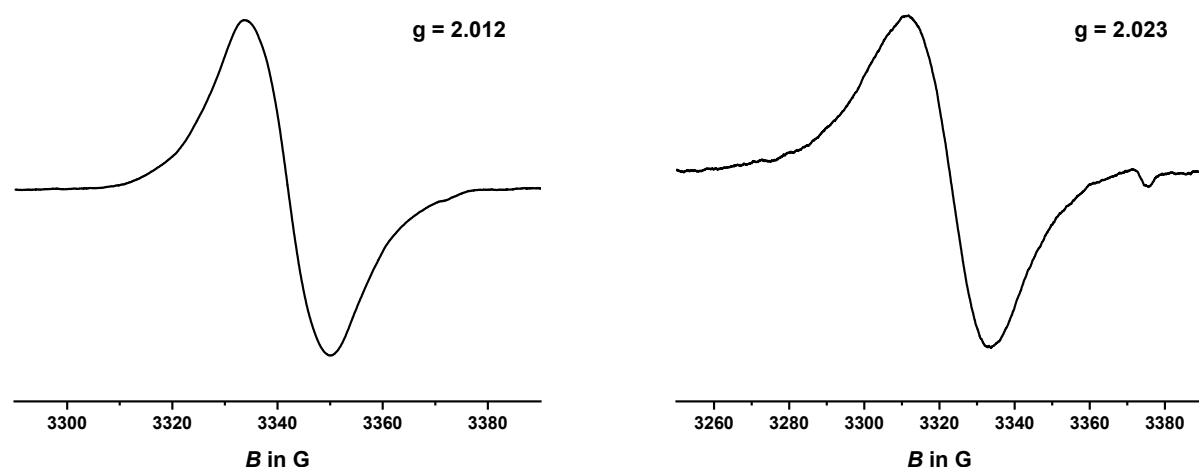
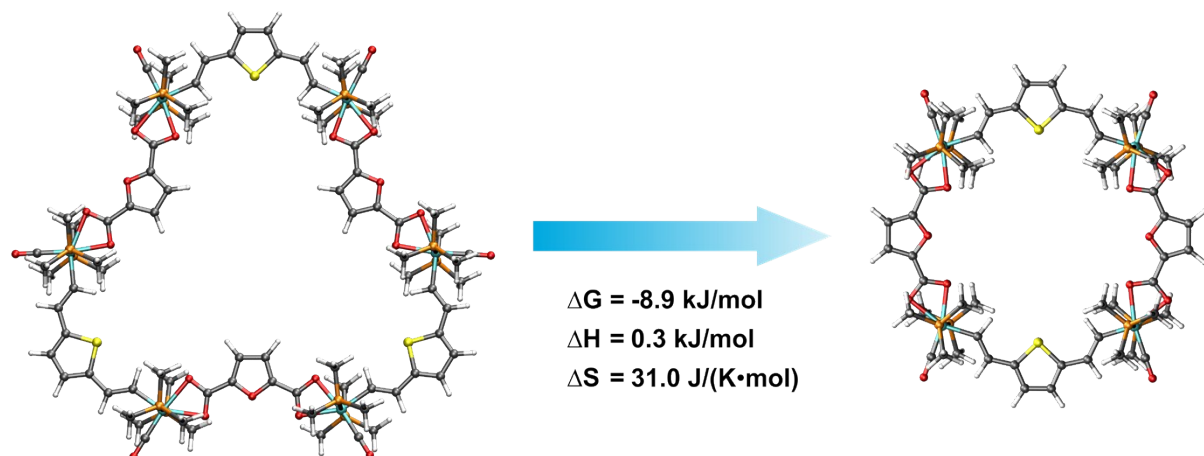


Figure S27. EPR spectra of  $\mathbf{2}\text{-TF}_4^{2+}$  (left) and  $\mathbf{2}\text{-TF}_4^{4+}$  (right) at room temperature.

## DFT Calculations



**Figure S28.** Calculated geometry-optimized structures of the two isomeric model compounds **2-TF<sub>4</sub>Me** (left) and **2-TF<sub>6</sub>Me** (right). Thermodynamic parameters are given per divinylthiophene diruthenium unit.

## References

- (1) Werner, H.; Esteruelas, M. A.; Otto, H. *Organometallics*, **1986**, 5 (11), 2295-2299.
- (2) Pfaff, U.; Hildebrandt, A.; Korb, M.; Oßwald, S.; Linseis, M.; Schreiter, K.; Spange, S.; Winter, R. F.; Lang, H. *Chem. Eur. J.*, **2016**, 22 (2), 783-801.
- (3) Dolomanov, O.V.; Bourhis, L. J.; Gildea, R. J.; Howard, J. A. K.; Puschmann, H. *J. Appl. Cryst.*, **2009**, 42 (2), 339-341.
- (4) Burla, M.C.; Caliandro, R.; Camalli, M.; Carrozzini, B.; Cascarano, G.L.; De Caro, L.; Giacovazzo, C.; Polidori, G.; Siliqi, D.; Spagna, R. *J. Appl. Cryst.*, **2007**, 40, 609-613.
- (5) Sheldrick, G.M. *Acta Cryst.* **2015**, A71, 3-8.
- (6) Sheldrick, G.M. *Acta Cryst.* **2015**, C71, 3-8.
- (7) Krejcik, M.; Danek, M.; Hartl, F. *J. Electroanal. Chem.*, **1991**, 317, 179-187.
- (8) Gaussian 09, Revision D.01, Frisch, M. J.; Trucks, G. W.; Schlegel, H. B.; Scuseria, G. E.; Robb, M. A.; Cheeseman, J. R.; Scalmani, G.; Barone, V.; Petersson, G. A.; Nakatsuji, H.; Li, X.; Caricato, M.; Marenich, A.; Bloino, J.; Janesko, B. G.; Gomperts, R.; Mennucci, B.; Hratchian, H. P.; Ortiz, J. V.; Izmaylov, A. F.; Sonnenberg, J. L.; Williams-Young, D.; Ding, F.; Lipparini, F.; Egidi, F.; Goings, J.; Peng, B.; Petrone, A.; Henderson, T.; Ranasinghe, D.; Zakrzewski, V. G.; Gao, J.; Rega, N.; Zheng, G.; Liang, W.; Hada, M.; Ehara, M.; Toyota, K.; Fukuda, R.; Hasegawa, J.; Ishida, M.; Nakajima, T.; Honda, Y.; Kitao, O.; Nakai, H.; Vreven, T.; Throssell, K.; Montgomery Jr. J. A.; Peralta, J. E.; Ogliaro, F.; Bearpark, M.; Heyd, J. J.; Brothers, E.; Kudin, K. N.; Staroverov, V. N.; Keith, T.; Kobayashi, R.; Normand, J.; Raghavachari, K.; Rendell, A.; Burant, J. C.; Iyengar, S. S.; Tomasi, J.; Cossi, M.; Millam, J. M.; Klene, M.; Adamo, C.; Cammi, R.; Ochterski, J. W.; Martin, R. L.; Morokuma, K.; Farkas, O.; Foresman, J. B.; Fox, D. J. Gaussian, Inc., Wallingford CT, **2016**.
- (9) Cossi, M.; Rega, N.; Scalmani, G.; Barone, V. *J. Comput. Chem.* **2003**, 24 (6), 669-681.
- (10) (a) Dolg, M.; Stoll, H.; Preuss, H. *J. Chem. Phys.* **1989**, 90 (3), 1730-1734; (b) Küchle, W.; Dolg, M.; Stoll, H.; Preuss, H. *J. Chem. Phys.* **1994**, 100 (10), 7535-7532.
- (11) Andrae, D.; Haeussermann, U.; Dolg, M.; Stoll, H.; Preuss, H. *Theor. Chim. Acta* **1990**, 77 (2), 123-141.
- (12) Hariharan, P. H.; Pople, J. A. *Theor. Chim. Acta* **1973**, 28 (3), 213-222.
- (13) (a) Perdew, J. P.; Burke, K.; Enzerhof, M. *Phys. Rev. Lett.* **1996**, 77 (18), 3865-3868; (b) Adamo, C.; Barone, V. *J. Chem. Phys.* **1999**, 110 (13), 6158-6170.
- (14) O'Boyle, N. M.; Tenderholt A. L.; Langner, K. M. *J. Comp. Chem.*, **2008**, 29 (5), 839-845.
- (15) Hanwell, M. D.; Curtis, D. E.; Lonie, D. C.; Vandermeersch, T.; Zurek E.; Hutchison, G. R. "Avogadro: An advanced semantic chemical editor, visualization, and analysis platform", *J. Cheminf.* **2012**, 4, 17.
- (16) Tange, O. *login: The USENIX Magazine*, **2011**, 36, 42-47.
- (17) Humphrey, W.; Dalke, A.; Schulten, K. *J. Mol. Graph.* **1996**, 14 (1), 33-38.
- (18) Persistence of Vision Pty. Ltd. (2004). Persistence of Vision Raytracer (Version 3.7), retrieved from <http://www.povray.org/download/>.